CHAPTER 6

Removal of Cd (II), Cr (VI) and Pb (II) by using chitosan coated *Citrus limetta* peels biomass in synthetic wastewater

Chapter 6: Removal of Cd (II), Cr (VI) and Pb (II) by using chitosan coated *Citrus limetta* peels biomass in synthetic wastewater

6.1.0 Introduction

Express industrialization and urbanization are the major sources of environmental pollutions [Claxton et al., 1998]. Various industrial activities like coal and petroleum refining, metal extraction and finishing, and leather processing generate large amount of hazardous effluents [Singh et al., 2020]. Industrial effluents contain large amount of heavy metal ions such as As^{+3}, Pb^{+2}, Cd^{+2}, Hg^{+2}, Cu^{+2}, Zn^{+2}, Ni^{+2} and Cr^{+6}. These toxic metal ions are responsible for various types of diseases in human beings [Dhal et al. 2013]. Cr (VI), Cd (II) and Pb (II) are on 17th, 7th, and 2nd position in ASTDR's priority list (https://www.atsdr.cdc.gov/spl/index.html). It has been observed that high level of heavy metal ions in the drinking water and food, damages liver and kidney and its low level causes skin problems, ulcer in the mucosal region, cancer in lungs and abdomen [Ray, 2016]. Therefore, discharge of heavy metal ions containing effluents into aquatic system must be regulated before it is discharged into natural water streams [Mitra et al., 2017].

Variety of techniques are used in heavy metal elimination from aqueous medium such as electrocoagulation [Bhatti et al. 2009], chemical reduction [Choudhary et al., 2017], filtration, membrane filtration [Jamshidifard et al., 2019], reverse osmosis [Mnif et al., 2017] and ion exchange [Petruzzelli et al., 1995]. These methods have several disadvantages like generation of toxic secondary sludge, operationally expensive and incomplete removal of heavy metals [Saha et al. 2013]. Therefore, an eco-friendly and inexpensive method of heavy metal removal is needed to be developed [Qasem et al., 2021]. Biomass such as plant, microbial and agro-waste have gained attention of researchers due to its inexpensive, ecofriendly, easily

and readily available (Qasem et al., 2021) in large quantity [Mahato et al., 2020; Ahmad and Zaidi, 2020] and contain huge quantity of cellulose, hemicellulose and lignin [Tursi, 2019]. Biomass has effective heavy metal removal efficiency due to presence of large amount of carbon which offers porous and irregular surface. Several low-cost biomass materials such as potato and banana peels [Mutongo et al., 2014, Ali et al., 2016], biodiesel waste residue [Muthusamy et al. 2014], etc. have been used for removal of heavy metal ions. *Citrus limetta* peel (CLP) is a readily and easily available fruit waste. It is a very common fruit in the India and other countries such as Brazil, China, United States and Mexico (https://www.worldatlas.com/articles/the-world-s-top-citrus-producing-countries.html). Food processing industries use *Citrus limetta* for the production of juice, jams, jellies and squashes. These units generate massive volume of *Citrus limetta peels* (CLP) as a waste. Sirajudeen et al., 2013 reported CLP as an effective biosorbent for the removal of heavy metal ions. Adhikari et al., 2017 reported that chemically modified CLP showed better heavy metal adsorption as compared to unmodified CLP.

Chitosan is a biopolymer considered as biodegradable and renewable material for the surface modification of biomass. Ample number of amino and hydroxyl groups form backbone of chitosan and these functional groups responsible for affinity of chitosan with heavy metal ions [Wu et al., 2010]. Coating of chitosan renders adsorbent's surface more porous and rough which enhances the surface area for adsorption [Ali et al., 2018]. The functional groups present on the biosorbents are actively involved in the adsorption of heavy metal ions. The present study aims at synthesis of cost effective and eco-friendly biosorbent for bioconversion-cum-biosorption of Cr (VI).

With these facts, the present investigation aimed at development of Chitosan coated *Citrus limette* peel (ChCLP) for simultaneous biosorption of Cr (VI), Cd (II) and Pb (II) in single and ternary metal ion system in the liquid phase. The surface morphology of ChCLP

was investigated by using SEM analysis. The elemental compositions on ChCLP surface and heavy metal binding on it was studied by EDX and elemental mapping. The surface functional groups on ChCLP surface were studied using FTIR. XPS study was performed to confirm heavy metal binding and reduction of Cr (VI) to Cr (III) on the ChCLP. Experimental data were fitted into various isotherm, thermodynamic, kinetic, dimensionless number and ANN modeling to understand the removal mechanism of heavy metal ions in single and ternary metal ion system.

6.2.0 Characterization of the ChCLP

The surface morphology, roughness and surface structure of ChCLP was characterized by using SEM and AFM. Elemental composition was analyzed by EDX, elemental mapping and XPS. FTIR and pH_{pzc} were used to elucidate the surface functional groups and pH on the ChCLP surface.

6.2.1 Surface morphological of chitosan coated *Citrus limetta* peels biomass

The SEM images of CLP, ChCLP, ChCLP-Cr(VI), ChCLP-Pb(II), ChCLP-Cd(II) and ternary metal ion system are shown in Figure 6.1.

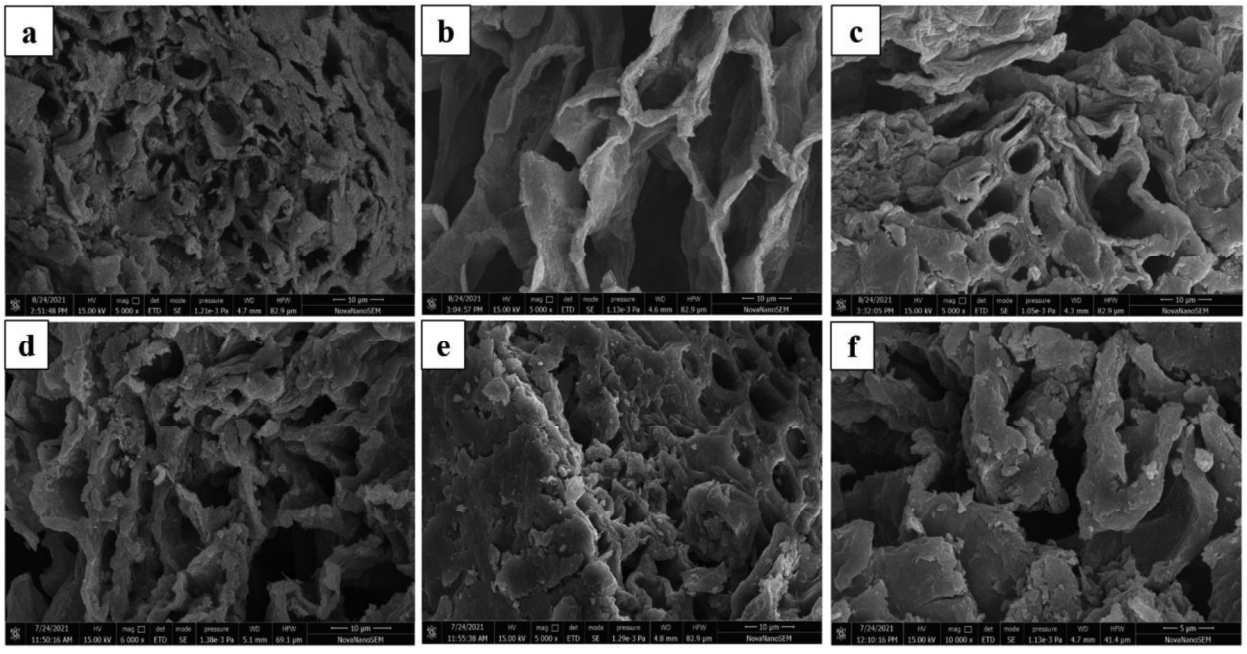

Figure 6.1. SEM image of CLP (**a**), ChCLP (**b**), ChCLP-Cr(VI) (**c**), ChCLP-Pb (**d**), ChCLP-Cd(II) **(e)** and ChCLP-Cr(VI)-Cd(II)-Pb(II) **(f).**

It is evident from SEM analysis (Figure 6.1a) that pores are present on the CLP surface. It also indicated rough surface, which might have provided enough space for binding of Cr (VI). SEM image of ChCLP is shown in Figure 6.1b. The surface morphology including pores and irregular structure was also observed in the Figure 6.1b similar to 1a. Figure 6.1c, d, and e indicate the ChCLP loaded with Cr (VI), Pb (II), Cd (II) in the single metal ion system. Figure 6.1f shows the Cr (VI), Cd (II) and Pb (II) adsorption on ChCLP surface in the ternary metal ion system. The comparative SEM study showed the changes in surface morphology of ChCLP before (Figure 6.1b) and after Cr (VI), Pb (II) and Cd (II) adsorption in single (Figure 6.1c-e), and ternary (Figure 6.1f) metal ion system. The pore structures were deformed and decreased roughness was observed in the Figure 6.1c-f. Mondal et al., 2019 investigated Cr (VI) removal by CLP and reported that rough surface of CLP became smooth after Cr (VI) adsorption. Owalude and Tella, 2016 investigated Cr (VI) adsorption by modified groundnut hull biomass and reported that the surface of biomass became smooth after the Cr (VI) loading. Tejada et al., 2021 performed adsorption of Pb (II) and Ni (II) in binary metal ion system by lemon peels. Authors investigated SEM analysis and confirmed changes in surface morphology of lemon peels biomass after adsorption. Adebayo et al., 2016 prepared activated carbon form orange peels for removal of Cd (II) and investigated SEM analysis for surface morphology. Authors reported micro porous structure surface of adsorbent which was suitable for Cd (II) adsorption.

6.2.2 Energy dispersive X- ray analysis and elemental mapping

The presence of major elements like O, C and N, and heavy metals (Cr (VI), Cd (II) and Pb (II)) adsorption on the ChCLP were determined by EDX (Figure 6.2).

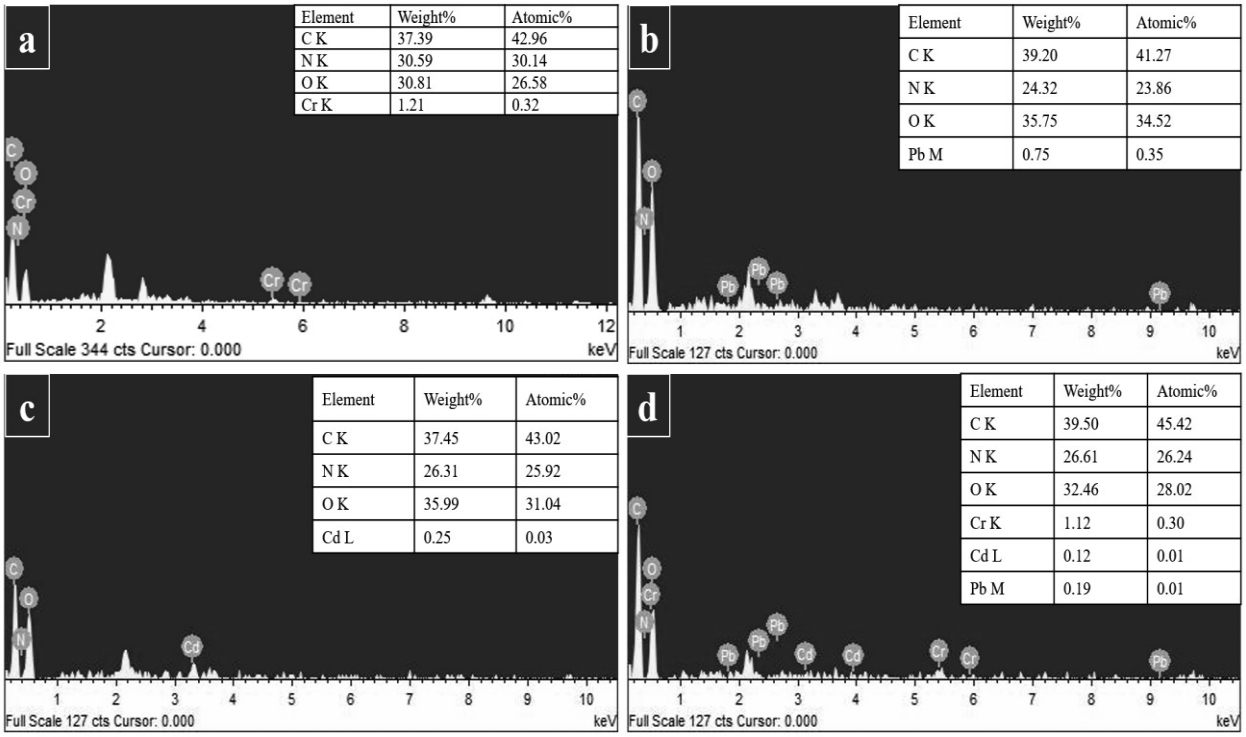

Figure 6.2. The EDX analysis of selected spectrum area of ChCLP-Cr (VI) **(a),** ChCLP-Pb(II) **(b),** ChCLP-Cd(II) **(c)** and ChCLP-Cr(VI)-Pb(II)-Cd(II) **(d).**

The C, N and O were observed as major elements in ChCLP (Figure 6.2). Figure 6.2 a, b and c specifies presence of Cr (VI), Pb (II) and Cd (II) on ChCLP surface revealed adsorption of heavy metal ions in single metal system. Figure 6.2 d designates the adsorption of ternary metal ions Cr (VI), Pb (II) and Cd (II) on the ChCLP surface in the ternary metal ion system. Altun, 2019 performed SEM-EDX of Cr (VI) loaded chitosan modified sour cherry kernel shell and reported the successful adsorption of Cr (VI) on the adsorbent. Tejada et al., 2021 investigated Pb (II) and Ni (II) adsorption on lemon peels biomass and confirmed adsorption of Pb (II) and Ni (II) on the adsorbent surface. Burk et al., 2020 investigated Cd (II) adsorption by chitosan coated biochar and reported presence of Cd (II) on the adsorbent's surface after Cd (II) adsorption. Madala et al., 2017 reported the presence of Cd (II) in the EDX analysis on the surface of chitosan coated adsorbent, which confirmed the adsorption of Cd (II). The presence of C, N, O and

heavy metal ions on ChCLP in EDX analysis was also confirmed through elemental mapping (Figure 6.3).

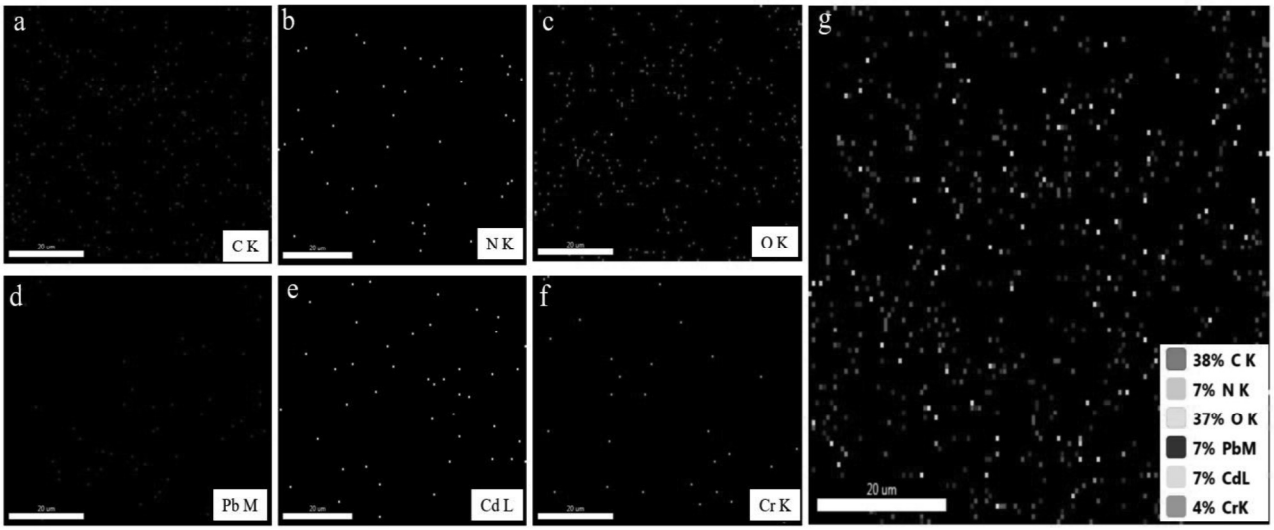

Figure 6.3. Elemental mapping of C (**a**), N (**b**), O (**c**), Pb (**d**), Cd (**e**), Cr (**f**) and percentage wise distribution of all ternary metal ions including C, N and O (**g**).

Large amount of C, O and N was observed in the elemental mapping (Figure 6.3 a, b and c). The presence of C and O made ChCLP a suitable adsorbent for Cr (VI) removal [Kibani et al., 2017]. Additionally, N was also present in higher quantity due to chitosan coating and it was responsible for the presence of surface functional groups like $–NH_2$. The homogeneous distribution of Pb (II) (Figure 6.3 d), Cd (II) (Figure 6.3 e) and Cr (VI) (Figure 6.3 f) on the ChCLP after adsorption was also reported in elemental mapping. Figure 6.3g indicates to the homogeneous distribution of ternary metal ions on the surface of ChCLP. Figure 6.3 g also revealed percentage wise distribution of Cr (4%), Cd (7%) and Pb (%) on the surface of ChCLP which shows the minimum adsorption of Cr (VI) and maximum adsorption of Pb (II) and Cd (II) on the adsorbent surface. Dewage et al., 2018 synthesized Pb (II) removal by chitosan modified biochar. Authors reported presence of nitrogen on chitosan coated biochar which indicated to chitosan coating on biochar. Dinh et al., 2020b performed the SEM elemental mapping of chitosan-MnO_2 nanocomposite and reported similar kind of results. Burk et al., 2020

performed elemental mapping of chitosan coated biochar after Cd (II) adsorption and revealed to the distribution of Cd (II) on chitosan coated biochar.

6.2.3 Fourier transformation infra-red analysis

The FTIR spectra of CLP, Chitosan, ChCLP and ChCLP-Cr (VI), ChCLP-Pb (II), ChCLP-Cd (II) and ternary metal ion-ChCLP are shown in Figure 6.4.

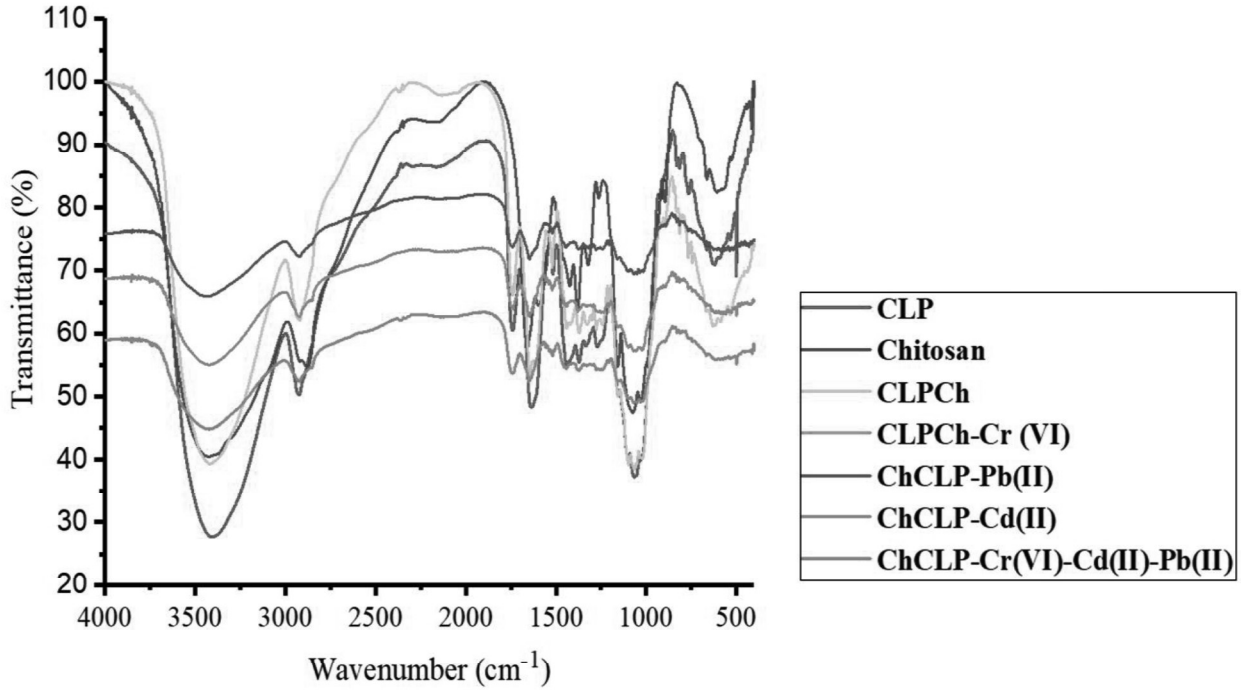

Figure 6.4. FTIR spectra of CLP, chitosan, ChCLP and ChCLP-Cr (VI), ChCLP-Cd (II), ChCLP-Pb (II) in single and ternary metal ion system.

The peaks of all samples between 3300-3500 cm^{-1} indicated O-H bonding. Vibrations at 2900-3000 cm^{-1} represented aliphatic C-H groups. FTIR peaks at 1659 cm^{-1} and 1597 cm^{-1} showed amide stretching vibration of –NHCO- and N-H of the $–NH_2$ group [Dinh et al., 2018]. The presence of $–NH_2$ group epitomized chitosan in the ChCLP [Zhang et al., 2018]. The spectral peak at 1084 cm^{-1} depicted –C-N stretching [Yadav et al. 2014]. There was broadness in the peaks of ChCLP as compared to CLP. The shifting in the FTIR spectra was due to the chitosan coating. Chitosan coating was responsible for enhanced $-NH_2$ groups on the adsorbent's surface which increases its adsorption property. There is a flatness in the FTIR

spectrum of Cr (VI), Cd (II), Pb (II) in single and ternary metal ion system loaded ChCLP, which represented heavy metal adsorption was mediated by its coordination with functional groups [Kibami et al., 2017]. Shrestha, 2016 obtained FTIR spectra of activated carbon fiber obtained from coconut shell and reported similar kind of results. Coates, 1996 also reported that the functional groups present on the biosorbent's surface were actively involved in the heavy metal removal. Schiewer and Balaria, 2009 investigated Pb (II) adsorption onto *Citrus* peels and reported that carboxyl groups of *Citrus* peels participated in the adsorption of Pb (II). Madala et al., 2017 investigated comparative FTIR analysis before and after Cd (II) adsorption onto chitosan coated ceramic and reported changes in the FTIR spectra after heavy metal adsorption.

6.2.4 Determination of pH range through point zero charge

The value of pH_{pzc} of ChCLP is shown in Figure 6.5.

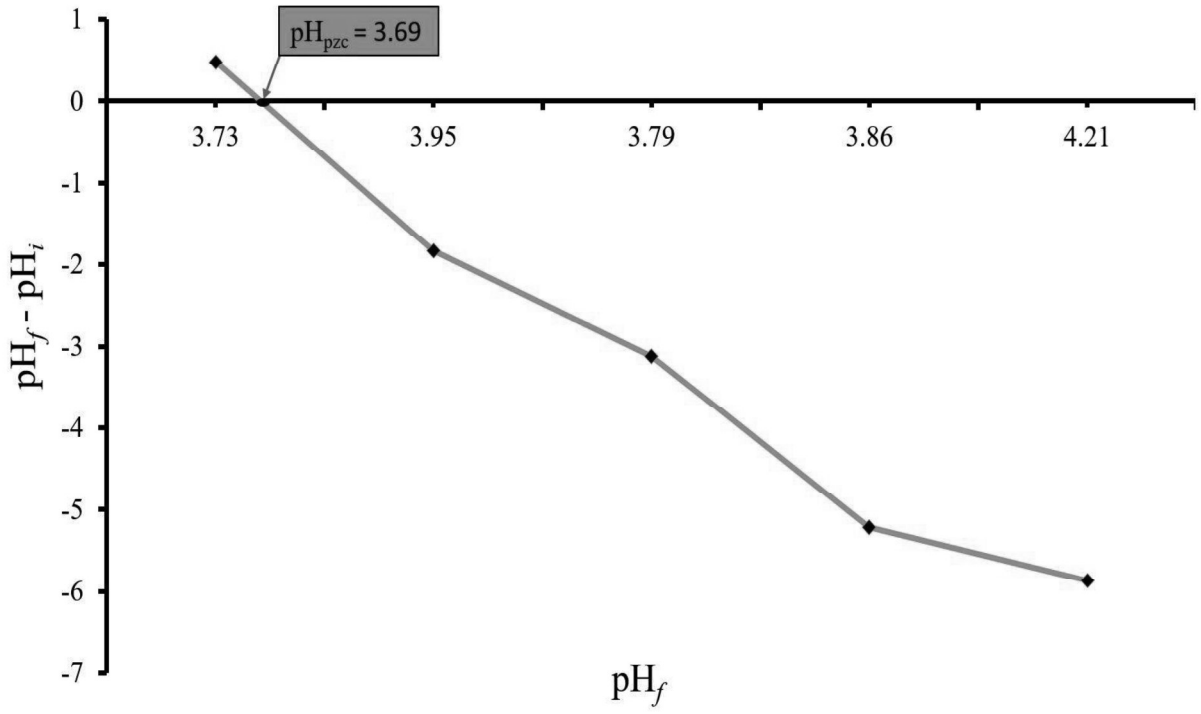

Figure 6.5. pH value at point zero charge (pH_{pzc}) of ChCLP

The value of pH_{pzc} was determined to be 3.69 (Figure 6.5). This indicated that Cr (VI) adsorption on the ChCLP was favored at the pH value lower than 3.69 and adsorption of Cd (II) and Pb (II) was favored at pH > 3.69 [Nomanbhay and Palanisamy, 2005]. The favorable Cr (VI) adsorption at lower pH was due to higher electrostatic attraction between surface functional groups (protonated) and chromate ions. The Cr (VI) ions exist as $HCrO_4^{2-}$ at acidic pH and adsorbed on the surface of ChCLP (Siboni et al. 2011). At lower pH, the surface of ChCLP was heavily protonated, which led to competition for binding site between excess hydrogen ions (H^+) and positive charged Pb (II) and Cd (II). With the increase in pH, the concentration of hydrogen ions decreased that led to increased Cd (II) and Pb (II) adsorption up to a limit [Petrovic et al., 2016]. Jayan et al., 2021 investigated Pb (II) and Zn (II) adsorption on PKM-2 *Moringa Oleifera* leaves. Authors investigated pH_{pzc} of PKM-2 *Moringa Oleifera* leaves and reported as 5.6. Srivastava et al., 2011 calculated pH_{pzc} (3.0) of *Mucor heimalis* biomass and authors reported maximum Cd (II) adsorption was achieved at pH 6.0 which was much higher than pH_{pzc} (3.0).

6.2.5 Atomic Force Microscopy

AFM images in 2 and 3 D of CLP and ChCLP are shown in Figure 6.6.

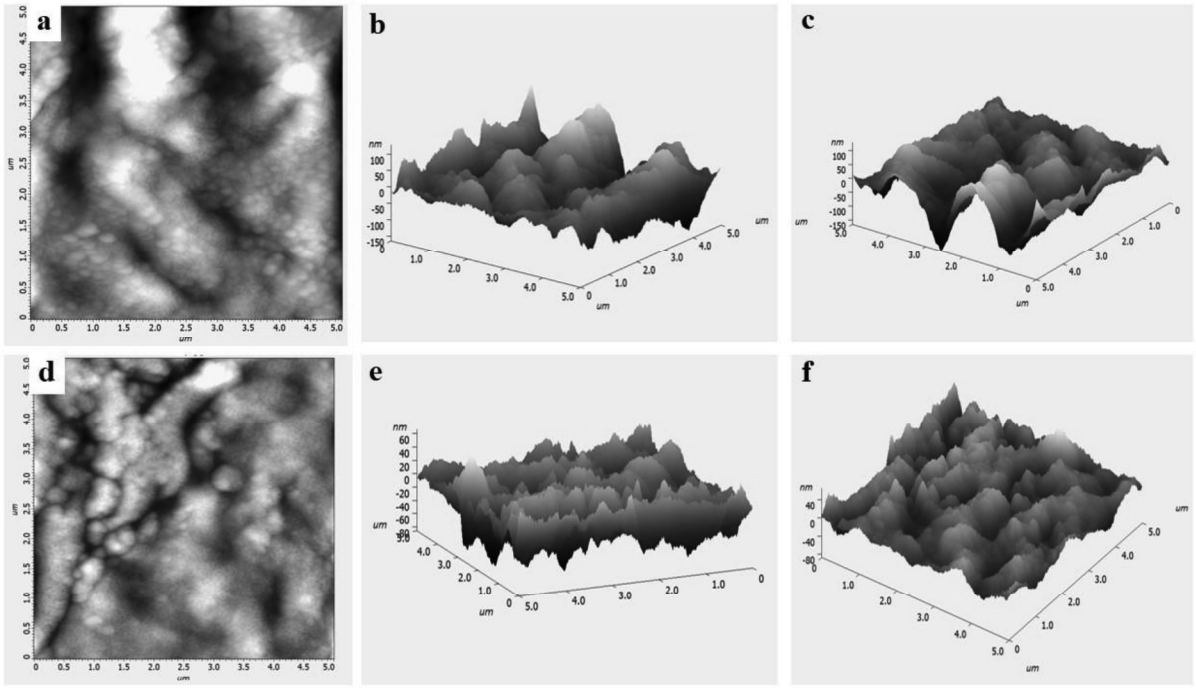

Figure 6.6. AFM image of CLP in 2-D (a) and 3-D (b, c). AFM images of ChCLP in 2-D (d) and 3-D (e, f).

The AFM images showed the morphological differences such as roughness, porosity and texture of CLP and ChCLP. The black and bright areas (Figure 6.6 a) in the AFM micrograph indicate grooves and extruded surface of CLP, respectively. The 2-D micrograph (Figure 6.6 d) of ChCLP indicated more grooves as compared to CLP. The surface roughness in the 2-D imaging was observed much higher in the ChCLP (13.06 nm) as compared to CLP (9.73 nm). Figure 6.6 b and c represent the AFM images of CLP in the 3-D. 3-D images of ChCLP are shown in Figure 6.6 e and f. More irregular and unequal surface of ChCLP was also observed as compared to CLP in the 3-D. The 3-D roughness of ChCLP was observed as 146.62 nm which was higher than that of CLP (28.62 nm). The increased roughness on the surface of ChCLP was due to chitosan coating, which favored the heavy metal adsorption. The maximum area valley depth and peak height observed in the ChCLP was 872.12 and 789.85 nm, respectively. However, in case of CLP, maximum valley depth (166.15 nm) and peak height (130.12 nm) were less as compared to ChCLP. The enhanced peak height of ChCLP

surface was due to binding of chitosan biopolymer with the surface functional groups. Q. AL-Shemary et al., 2020 investigated Azure A dye adsorption on Snail shell and authors studied adsorbent surface roughness through AFM. Authors reported that modification of snail shell surface enhanced the roughness which resulted in increased adsorption of dye.

6.2.6 XPS

In the XPS analysis, the adsorption of Cr (VI), Cd (II) and Pb (II) on ChCLP in single and ternary metal ion system was confirmed. The XPS analysis of heavy metal adsorption is shown in Figure 6.7.

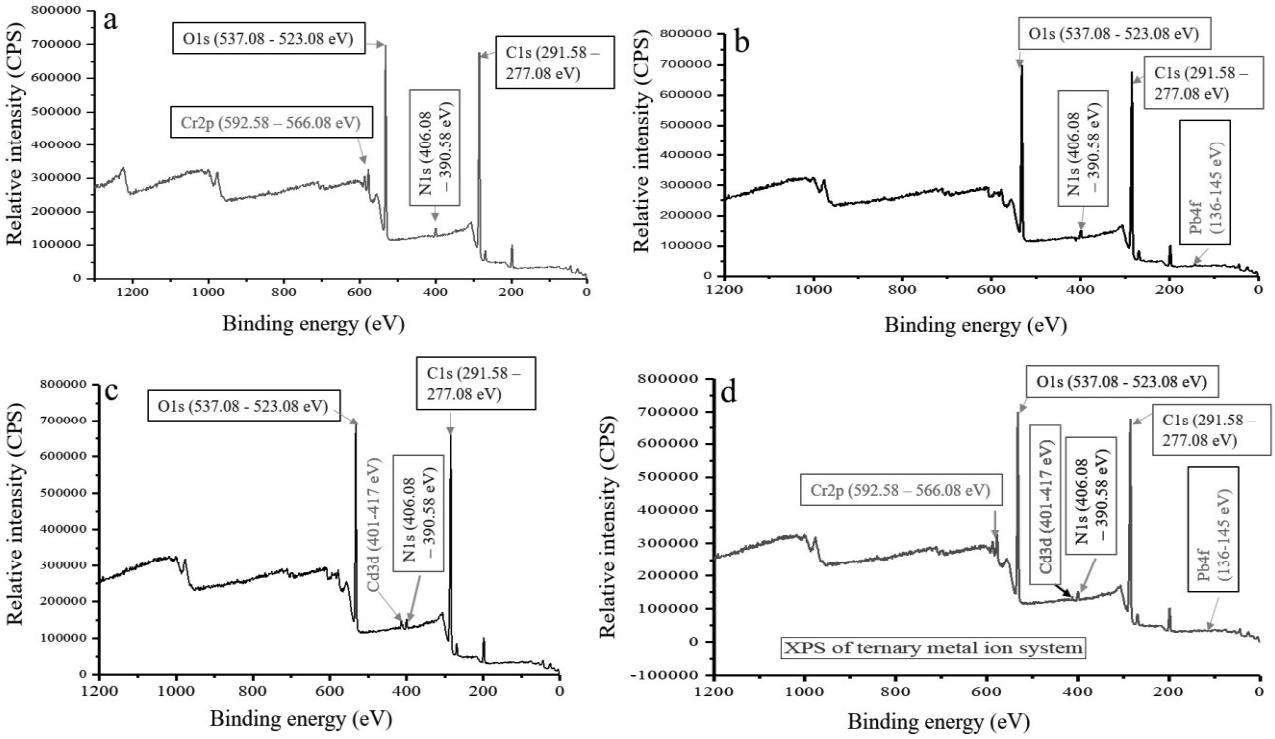

Figure 6.7. XPS spectra of ChCLP-Cr (VI) (**a**), ChCLP-Pb(II) (**b**), ChCLP-Cd(II) (**c**) of single and ternary (**d**) metal ion system.

The binding of Cr on the surface of ChCLP was observed at peaks generated between 592.58-566.08 eV (Figure 6.7a). Binding of Pb (II) on the surface of ChCLP was observed at binding energy between 136-145 eV (Figure 6.7b). Adsorption of Cd on the surface of ChCLP was confirmed through XPS at binding energy range of 401-417 eV (Figure 6.7c). The adsorption of Cr (VI), Cd (II) and Pb (II) in the ternary metal ion system was also confirmed

through XPS analysis (Figure 6.7d). Selvanantharajah et al., 2021 investigated Pb (II) removal by oxidized graphite and confirmed Pb (II) adsorption through XPS analysis. Zhang et al., 2020c reported adsorption of Cd (II) and Pb (II) adsorption on waste biomass based hydrogel and confirmed the binding of Cd (II) and Pb (II) in XPS analysis. Aranda-Garcia and Cristiani-Urbina, 2020 investigated chromium adsorption on *Quercus crassipes* (a corn shell biomass and confirmed chromium adsorption on the biomass surface through XPS analysis. The major peaks were of C and O. The N is the component of chitosan biopolymer and was also observed in this study. Daniyal et al., 2021 investigated XPS of Chitosan-Graphene Oxide-based composite. Authors reported sub-peaks at 399.2 eV and 400.2 eV, which indicated the presence of nitrogenous groups on chitosan. The reduction of Cr (VI) to Cr (III) on ChCLP was also studied and is shown in Figure 6.8.

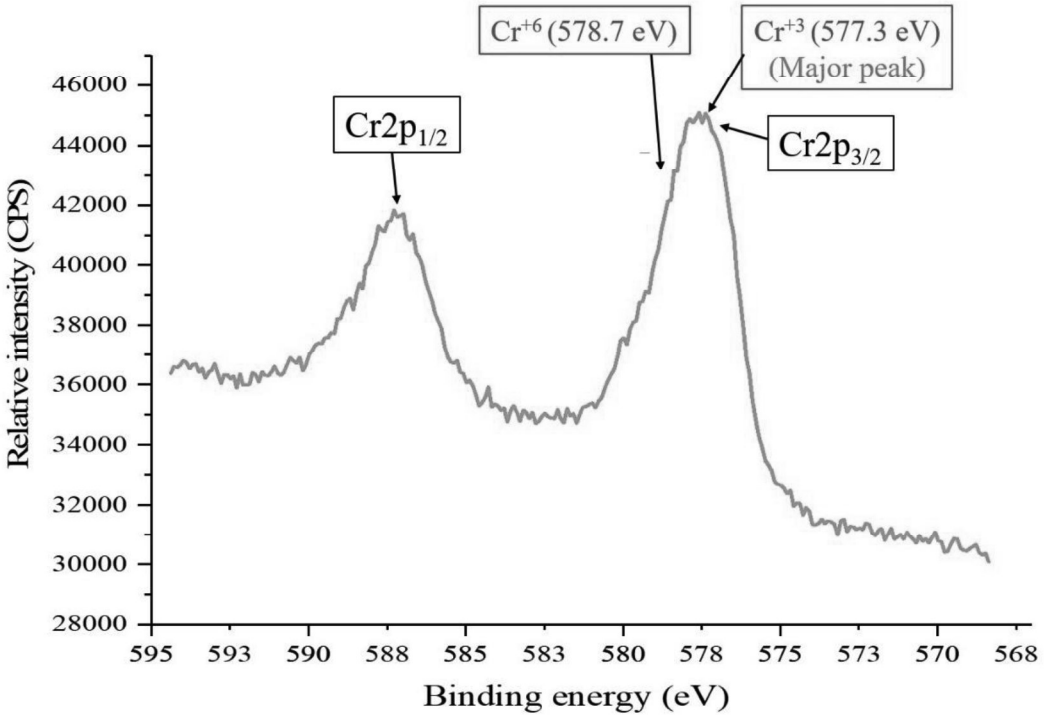

Figure 6.8. Biotransformation of Cr (VI) into Cr (III) on ChCLP

The conversion of Cr (VI) was also confirmed by XPS signals of Cr2p3/2. Cr2p3/2 contains both oxidation state of chromium between 592.58 to 566.08 eV. The major peak of Cr (III) was observed at 573.3 eV and minor peak region was occupied by Cr (VI) at 578.7 eV.

The major peak of Cr (III) clearly pointed out the fruitful bioconversion of Cr (VI) to Cr (III). Bandara et al., 2020 investigated the mechanism of Cr (VI) reduction by using grapheme-oxide-polymer and observed that redox reaction was involved in the conversion of Cr (VI) to Cr (III). Huang et al., 2016 obtained similar results by using modified walnut shell biochar as an adsorbent.

6.3.0 Adsorption study

6.3.1 Experimental parameter optimization

In the present study, experimental parameters such as pH, temperature, initial heavy metal ion concentration, ChCLP dosage, contact time and agitation rate were optimized. The results of parameter optimization for Cr (VI), Cd (II) and Pb (II) removal are shown in Figure 6.9, 6.10 and 6.11.

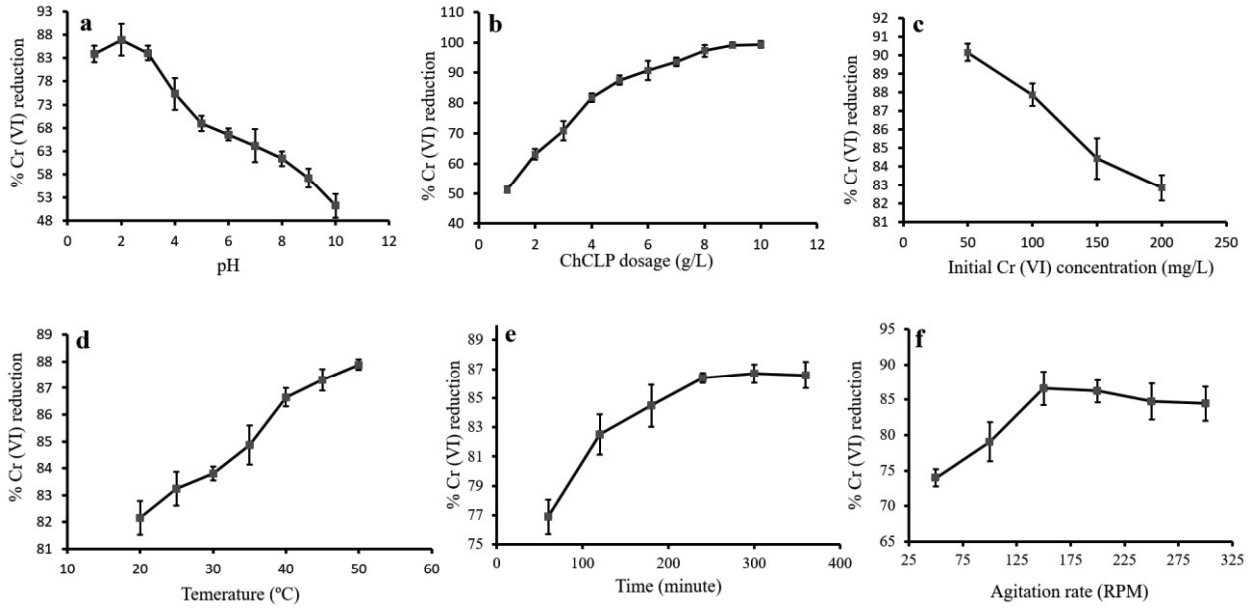

Figure 6.9 Effect of pH (a), ChCLP dosage (b), initial Cr (VI) concentration (c) reaction temperature (d), contact time (e) and agitation rate (f) on the Cr (VI) removal

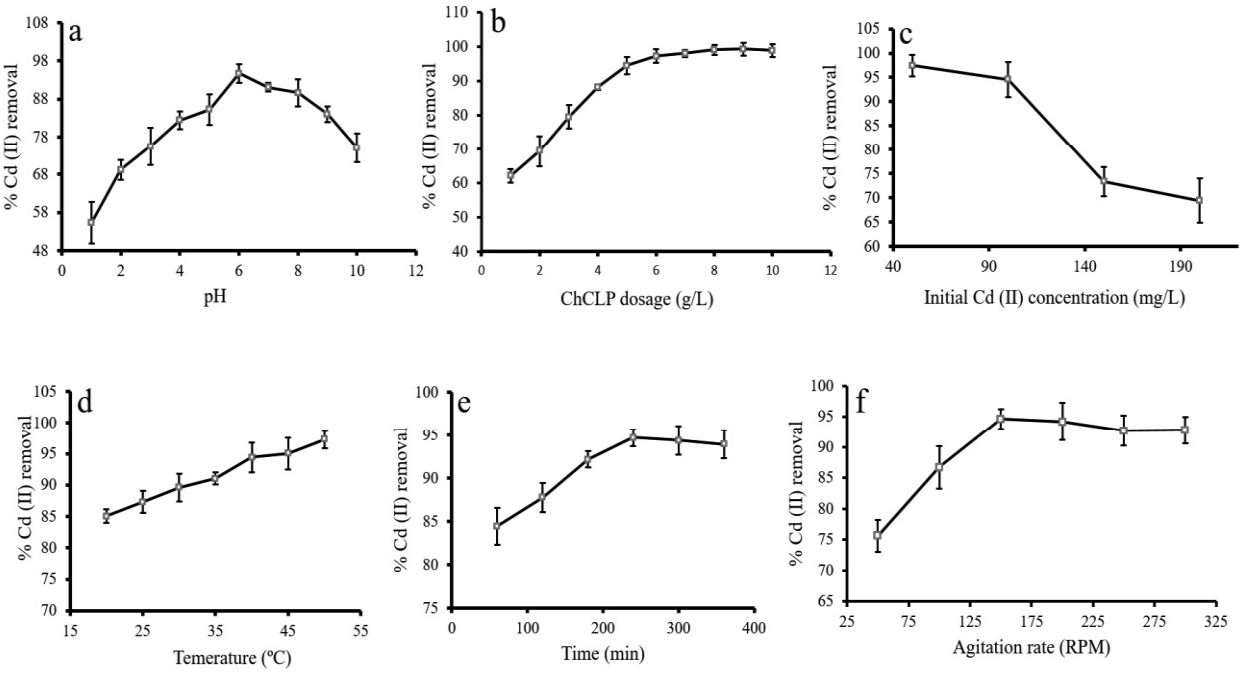

Figure 6.10 Effect of pH (a), ChCLP dosage (b), initial Cd (II) concentration (c), temperature (d), contact time (e), and agitation rate (f) on removal of Cd (II).

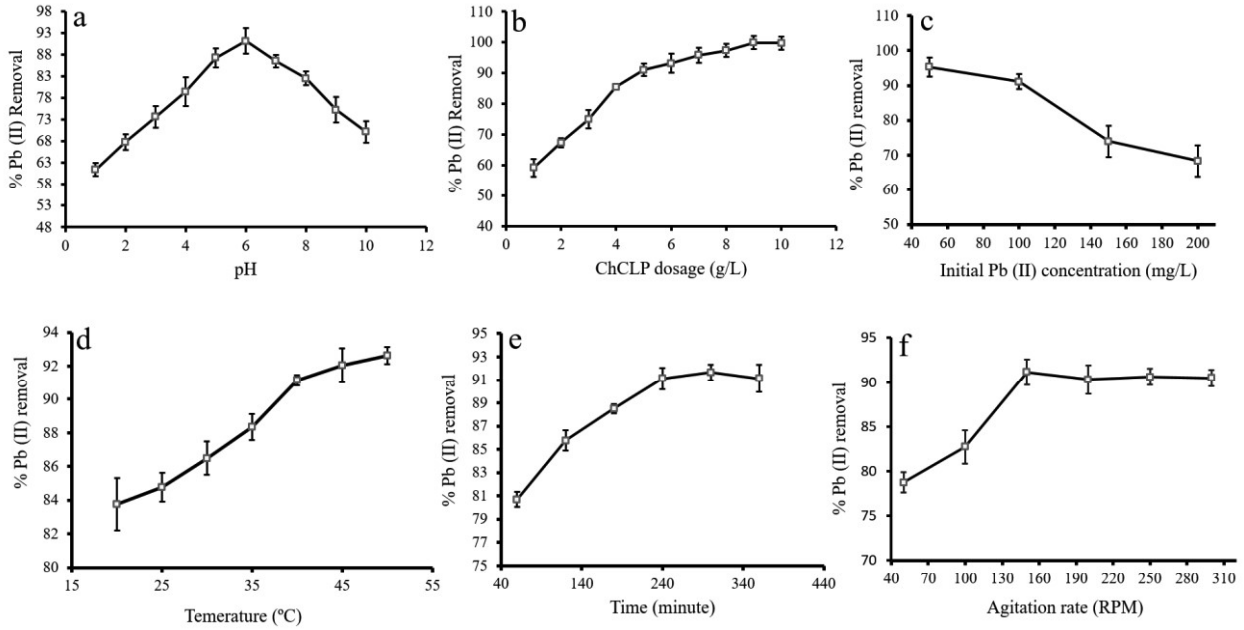

Figure 6.11 Effect of pH (a), ChCLP dosage (b), initial Pb (II) concentration (c), temperature (d), contact time (e), and agitation rate (f) on removal of Cd (II).

The pH for removal of Cr (VI), Cd (II) and Pb (II) was tested in the range of pH 1-10 whereas other parameters such as temperature (40ºC), initial heavy metal ion concentration (100 mg/L), ChCLP dose (5 g/L), reaction time (240 minutes) and agitation rate (150 rpm) were kept constant. The results showed that the maximum Cr (VI) removal was achieved at pH 2 (Figure 6.9 a). The Cr (VI) has several stable species such as CrO_4^{2-}, HCr^{4-} and $Cr_2O_7^{2-}$. The maximum Cr (VI) removal at acidic pH (pH 2) was achieved due to electrostatic attraction between negatively charged Cr (VI) and positively charged surface of ChCLP [Mondal and Roy, 2018]. However, at alkaline or higher pH, the surface of ChCLP is spiked with negative charge, which is unfavourable for adsorption of negatively charged Cr (VI) species [Khambhaty et al. 2009]. On other hand, the removal of Cd (II) and Pb (II) increased with increase in pH and maximum Cd (II) (Figure 6.10a) and Pb (II) (Figure 6.11a) removal was achieved at pH 6. At acidic pH, the hydrogen ions remain dominant in the solution and create competition between positive charged heavy metal ions (Cd^{2+} and Pb^{2+}) and H^+ for surface binding sites. Increasing the pH, the concentration of H^+ reduced in the solution and adsorption of Cd (II) and Pb (II) was increased at certain pH range (pH 6). Zhang et al., 2020 investigated removal of Cd (II) and Pb (II) using waste biomass based hydrogel and reported similar kind of effect of pH on adsorption of heavy metal ions. Kosa et al., 2012 also reported that Pb (II) adsorption increased with increase in pH up to 7.

The initial Cr (VI), Cd (II) and Pb (II) concentration in the solution was evaluated over a range of 50 to 200 mg/L. The Cr (VI), Cd (II) and Pb (II) removal decreased from 90.16 to 82.84% (Figure 6.9 c), 97.45 to 69.42 % (Figure 6.10c) and 95.31 to 68.35 % (Figure 6.11c), respectively with increase in concentration of initial heavy metal ion from 50 to 200 mg/L. The rationale behind decrease in percentage removal above 50 mg/L was the saturation of active sites at high concentration [Dinh et al., 2019]. Pakshirajan et al., 2013 performed Cr (VI) adsorption onto banana peels and have reported similar results. Manjuladevi et al., 2018

investigated Cr (VI), Cd (II), Ni (II) and Pb (II) removal by using activated carbon prepared from *Cucumis melo* peels and observed effect of initial metal ion concentration from 100 - 400 mg/L. Authors reported that maximum removal of heavy metal ions was achieved at 100 mg/L. Zhang et al., 2020 also reported similar kind effect of initial heavy metal (Cd and Pb) concentration on removal efficiency.

The effect of ChCLP dose was investigated between 1-10 g/L where pH 2 for Cr (VI) and pH 6 for Cd (II) and Pb (II), temperature (40ºC), initial heavy metal ion concentration (100 mg/L**),** agitation rate (150 rpm) and incubation time (240 minutes) were kept constant. The Cr (VI) exclusion increased from 51.23 to 99.34 % (Figure 6.9b), Cd (II) removal was increased from 62.12 to 98.91 % (Figure 6.10 b) and Pb (II) removal was increased from 59.16 to 99.80 % (Figure 6.11 b) with increase in ChCLP dose from 1 to 10 g/L. This indicates that abundance of ChCLP provided more surface area for heavy metal adsorption [Srividya and Mohanty, 2009]. Mondal et al., 2019 investigated Cr (VI) by mosambi peel biomass and obtained alike fallouts. Kalak et al., 2021 investigated Pb (II) removal by fly ash and reported maximum Pb (II) at 10 g/L adsorbent dosage. Moyo et al., 2013 also obtained similar kind of results during the removal of Pb (II) by using maize tessel based activated carbon. Hussain et al., 2020 investigated Cd (II) removal by using magnetic spent coffee biochar and reported removal of Cd (II) increased with increase in adsorbent dosage.

The heavy metal adsorption is highly dependent on the temperature [Alkan and Dogan, 2003, Salleh et al. 2011]. In the present investigation, Cr (VI), Cd (II) and Pb (II) removal increased from 82.15 to 87.88% (Figure 6.9 d), 85.06 to 97.31% (Figure 6.10 d) and 83.77 to 92.61% (Figure 6.11 d), respectively with increase in the temperature from 20 to 50°C. However, when temperature was increased above 50 ºC, the heavy metal removal decreased. Present study showed that Cr (VI), Cd (II) and Pb (II) adsorption on ChCLP was endothermic. The enhancement in heavy metal adsorption was might be due to activation of ChCLP surface

at higher temperature [Senthilkumar et al., 2006]. Dawodu et al., 2020 obtained similar outcomes while performing the removal of Cr (VI) on *Heinsia crinita* seed coat biomass. Madala et al., 2013 investigated Cd (II) removal using chitosan coated ceramic alumina and reported that Cd (II) adsorption was endothermic. Dewage et al., 2018 reported Pb (II) removal was favorable at higher temperature on the chitosan modified biochar.

Cr (VI) (Figure 6.9 e), Cd (II) (Figure 6.10 e) and Pb (II) (Figure 6.11 e) removal was investigated at various contact time in range of 60 to 360 minutes and other parameters remained constant during this study. Heavy metal removal on ChCLP was quick for initial 240 minutes. Thereafter, it slowed down. The maximum removal of Cr (VI) (86.69 %) and Pb (II) (91.65%) was achieved at 300 minutes. Maximum removal of Cd (II) (94.69%) was achieved at 240 minutes. Afterwards, there was no or negligible increment in heavy metal removal owing to occupancy of all active sites of ChCLP at 300 minutes for Pb (II) and Cr (VI), and 240 minutes for Cd (II) [Singh et al. 2021a]. Gupta et al., 2013 performed Cr (VI) removal by *Ficus carica* and observed that Cr (VI) adsorption increased continuously up to 210 minutes. The equilibrium was achieved at 210 minutes and thereafter, there was no increment in the Cr (VI) adsorption. Shofiyani et al., 2015 reported that Cd (II) removal increased with rise in time on chitosan modified chlorella biomass. Authors reported that Cd (II) removal quickly increased up to initial 30 minutes and thereafter removal rate became slowdown. Ahmad et al., 2018 investigated Pb (II), Cu (II) and Cd (II) removal using by biochar derived potassium rich biomass. Authors reported that heavy metal removal quickly increased up to initial 10 hours and after that removal of heavy metal became slow.

The effect of agitation rate on removal of Cr (VI) (Figure 6.9 f), Cd (II) (Figure 6.10 f) and Pb (II) (Figure 6.11 f) was investigated at various agitation rate ranging from 50-300 rpm. The removal of heavy metal ion increased with surge in agitation rate and maximum removal of Cr (VI), Cd (II) and Pb (II) was reported at 150 rpm. This increment in the removal

of heavy metal ions was due to the increase in turbulence in aqueous phase which resulted higher collision rate between ChCLP and metal ion and reduced thickness of boundary layer surrounding the ChCLP. Kumar and Jena, 2017 studied the effect of agitation rate on the removal of Cr (VI) using chemical activated $ZnCl_2$ nanoparticles. Authors concluded that % removal of Cr (VI) increased with the rise in agitation rate from 90 - 150 rpm and there was no effect on Cr (VI) adsorption above 150 rpm. Wadie and Al-Khawaja, 2018 investigated the removal of Cd (II) and Ag (I) on nano activated alumina. Authors reported that removal of Cd (II) and Ag (I) increased with increasing agitation rate. Badmus et al., 2007 reported that removal of Pb (II) on activated carbon prepared from Periwinkle Shells increased with escalation in agitation rate from 300-700 rpm and maximum removal of Pb (II) was achieved at 700 rpm.

6.3.2 Isotherm

The isotherm study of Cr (VI), Cd (II) and Pb (II) onto ChCLP was studied at various at temperature ranging from 20 to 50 ºC by varying initial metal ion concentration from 50 to 200 mg/L. The experimental data of single metal ion and ternary metal ion system were fitted in the Langmuir, Freundlich, Temkin and Halsey isotherm (Figure 6.12, 6.13, 6.14, 6.15 and 6.16).

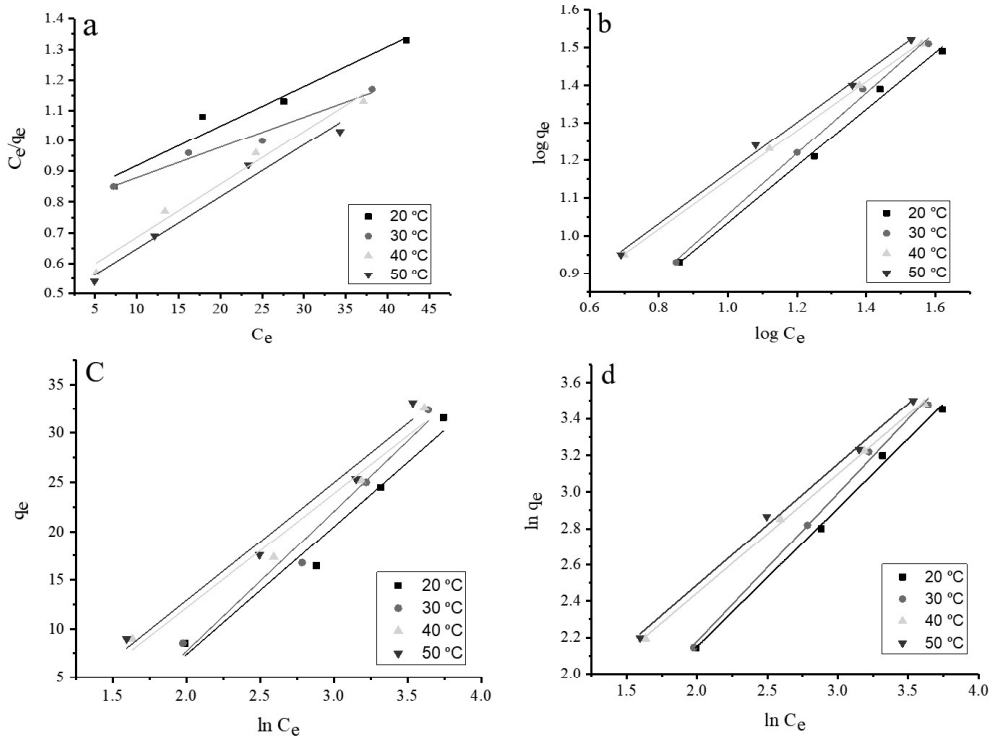

Figure 6.12 Langmuir (a) and Freundlich (b), Temkin (c) and Halsey (d) isotherm for Cr (VI) adsorption on ChCLP

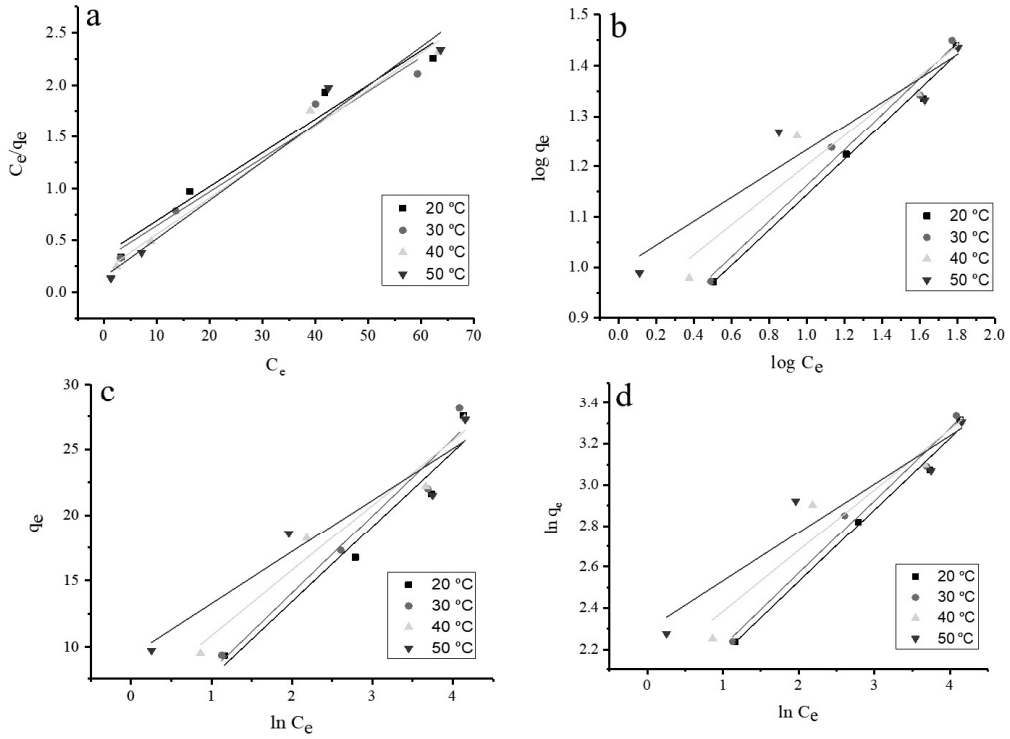

Figure 6.13 Langmuir (a) and Freundlich (b), Temkin (c) and Halsey (d) isotherm for Pb (II) adsorption on ChCLP

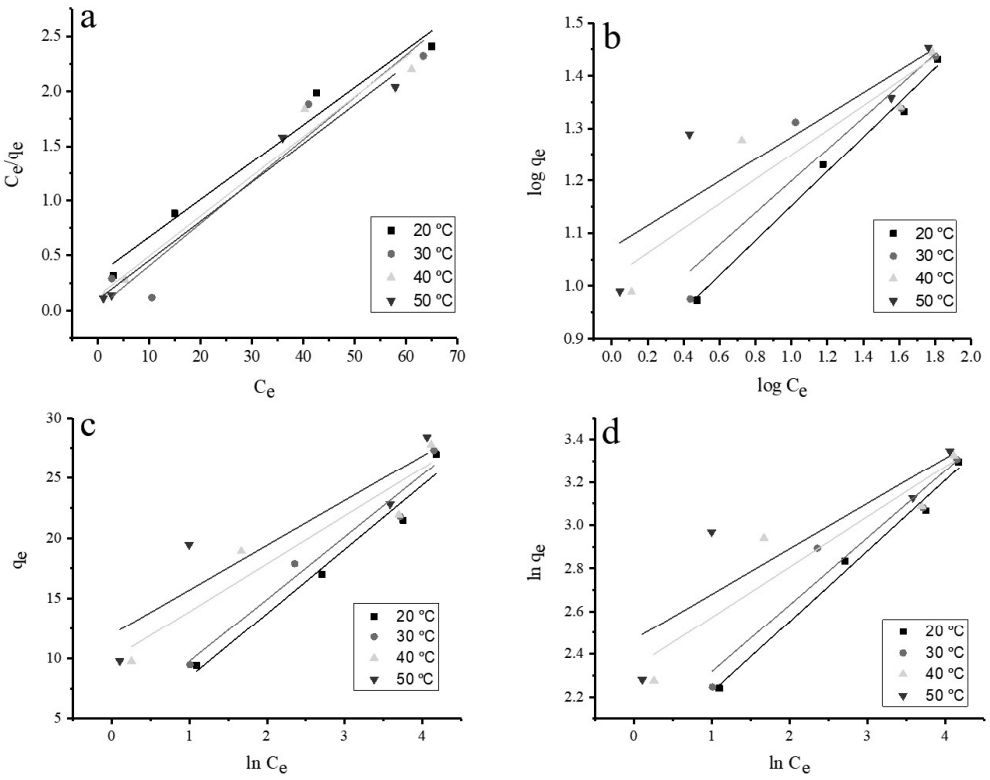

Figure 6.14 Langmuir (a) and Freundlich (b), Temkin (c) and Halsey (d) isotherm for Cd (II) adsorption on ChCLP

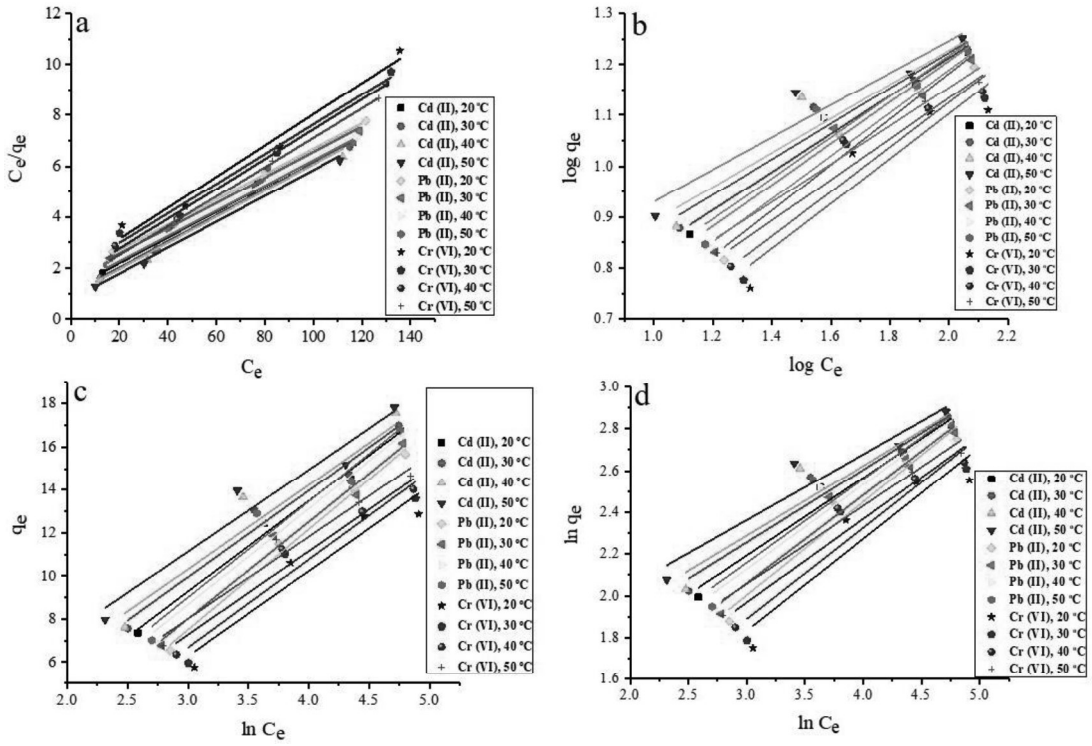

Figure 6.15 Langmuir (a) and Freundlich (b), Temkin (c) and Halsey (d) isotherm for adsorption of Pb (II), Cd (II) and Cr (VI) in ternary metal ion system on ChCLP

Parameters of Langmuir, Freundlich, Temkin and Halsey isotherm of single and ternary metal ion system were calculated from the slope and intercept of isotherm graphs. Cr (VI), Cd (II) and Pb (II) adsorption isotherm parameters were tabulated in the Table 6.1.

Table 6.1 Isotherm parameters of Cr (VI), Cd (II) and Pb (II) adsorption in single metal ion system

Metal	**Isotherms**	**Parameters**	**20ºC**	**30ºC**	**40ºC**	**50ºC**
Pb (II)	Langmuir	B	0.36	0.318	0.210	0.147
		Q^0	3.3×10^{-2}	3.2×10^{-2}	3.5×10^{-2}	3.7×10^{-2}
		R^2	0.98	0.98	0.99	0.98
		RSS	0.081	0.068	0.048	0.098
	Freundlich	k_f	0.349	0.353	0.295	0.236
		N	0.79	0.81	0.91	0.99
		R^2	0.95	0.96	0.93	0.92
		RSS	0.001	0.002	0.007	0.008
	Temkin	A_T	2.02	2.34	5.89	9.33
		b_T	5.69	5.85	4.94	3.92
		R^2	0.95	0.95	0.95	0.92
		RSS	8.59	7.69	4.94	3.92
	Halsey	K_H	0.34	0.35	0.29	0.24
		n_H	1.82	1.86	2.08	2.29
		R^2	0.99	0.98	0.93	0.92
		RSS	0.005	0.011	0.04	0.05
	Langmuir	B	1.3×10^{-2}	0.9×10^{-2}	1.7×10^{-2}	1.6×10^{-2}
		Q^0	0.78	0.77	0.51	0.47

Cr (VI)		R^2	0.95	0.97	0.98	0.97
		RSS	5.0×10^{-3}	1.0×10^{-3}	3.0×10^{-3}	4.0×10^{-3}
	Freundlich	k_f	0.75	0.80	0.65	0.67
		N	0.28	0.25	0.49	0.49
		R^2	0.99	0.99	0.99	0.99
		RSS	8.76×10^{-4}	5.98×10^{-4}	4.53×10^{-4}	5.34×10^{-4}
	Temkin	A_T	-18.74	-20.83	-11.20	11.12
		b_T	13.07	14.28	11.67	12.02
		R^2	0.96	0.97	0.97	0.97
		RSS	9.69	7.54	7.42	7.73
	Halsey	K_H	0.75	0.81	0.65	0.66
		n_H	0.63	0.55	1.14	1.16
		R^2	0.99	0.99	0.99	0.99
		RSS	3.1×10^{-3}	3.7×10^{-3}	8.43×10^{-2}	3.2×10^{-3}
Cd (II)		B	0.32	0.02	0.12	0.09
	Langmuir	Q^0	3.4×10^{-2}	4.1×10^{-2}	3.6×10^{-2}	3.5×10^{-2}
		R^2	0.98	0.97	0.98	0.98
		RSS	0.07	0.02	0.08	0.05
	Freundlich	k_f	0.32	0.30	0.23	0.21
		N	0.82	0.89	1.01	1.07
		R^2	0.95	0.86	0.87	0.78
		RSS	0.10	0.16	0.13	0.26
	Temkin	A_T	3.10	4.58	9.93	11.99
		b_T	5.32	5.17	3.97	3.71

		R^2	0.96	0.95	0.90	0.84
		RSS	5.32	7.00	16.51	28.96
	Halsey	K_H	0.32	0.31	0.23	0.21
		n_H	1.89	2.01	2.30	2.46
		R^2	0.95	0.94	0.87	0.78
		RSS	0.10	0.30	0.09	0.13

Isotherm study of Cr (VI), Cd (II) and Pb (II) was also investigated for ternary metal ion system. Isotherm study of ternary metal ion system was performed at 50-200 mg/L initial metal ion concentration of each metal and several temperature range of 20, 30, 40 and 50°C. The parameters of isotherms are tabulated in the Table 6.2.

Table 6.2 The isotherm parameters of Cr (VI), Cd (II) and Pb (II) in the ternary metal ion system.

Metal	**Isotherms**	**Parameters**	**20ºC**	**30ºC**	**40ºC**	**50ºC**
Pb (II)		B	1.70	1.56	1.35	1.26
	Langmuir	Q^0	0.04	0.05	0.04	0.05
		R^2	0.99	0.99	0.99	0.99
		RSS	0.02	0.03	0.04	0.01
		k_f	0.44	0.42	0.40	0.40
	Freundlich	N	0.28	0.34	0.39	0.41
		R^2	0.96	0.95	0.93	0.95
		RSS	0.13	0.14	0.15	0.17
	Temkin	A_T	-6.48	-5.49	-4.69	-4.36
		b_T	4.66	4.45	4.46	4.45

		R^2	0.98	0.98	0.96	0.94
		RSS	0.35	0.83	1.53	2.71
	Halsey	K_H	0.44	0.42	0.41	0.40
		n_H	0.66	0.79	0.91	0.95
		R^2	0.96	0.95	0.93	0.90
		RSS	0.11	0.21	0.21	0.20
Cd (II)		B	1.17	0.99	0.93	0.76
	Langmuir	Q^0	0.05	0.05	0.05	0.05
		R^2	0.99	0.99	0.99	0.99
		RSS	0.06	0.09	0.07	0.06
		k_f	0.37	0.34	0.33	0.31
	Freundlich	*N*	0.46	0.52	0.55	0.61
		R^2	0.97	0.94	0.93	0.88
		RSS	0.12	0.30	0.81	0.51
	Temkin	A_T	-3.35	-2.11	-1.42	-0.30
		b_T	4.21	4.01	3.91	3.81
		R^2	0.98	0.97	0.89	0.94
		RSS	0.42	1.26	5.24	2.75
	Halsey	K_H	0.37	0.34	0.33	0.31
		n_H	1.07	1.21	1.28	1.41
		R^2	0.97	0.94	0.88	0.92
		RSS	0.31	0.24	0.48	0.22
Cr (VI)		B	1.91	1.81	1.59	1.36
	Langmuir	Q^0	0.06	0.05	0.06	0.06

	R^2	0.95	0.94	0.96	0.94
	RSS	0.63	0.37	0.11	0.51
Freundlich	k_f	0.44	0.43	0.39	0.37
	N	0.22	0.25	0.33	0.40
	R^2	0.98	0.98	0.98	0.99
	RSS	0.01	0.09	0.05	0.04
Temkin	A_T	-5.57	-5.56	-4.36	-3.41
	b_T	3.95	4.08	3.87	3.80
	R^2	0.91	0.93	0.95	0.96
	RSS	2.89	2.45	1.42	1.14
Halsey	K_H	0.44	0.43	0.39	0.37
	n_H	0.51	0.57	0.76	0.93
	R^2	0.87	0.88	0.91	0.93
	RSS	0.15	0.14	0.31	0.22

The higher R^2 values and lower RSS indicated that Langmuir isotherm was best fitted in the adsorption of Pb (II) and Cd (II) in both single and ternary metal ion system. Suitability of Langmuir isotherm indicated monolayer adsorption of Cd (II) and Pb (II) on the homogeneous surface of ChCLP. Freundlich isotherm was best fitted in the adsorption of Cr (VI) in both single and ternary metal ion system on ChCLP. This represented the heterogeneous surface of ChCLP and multilayer Cr (VI) adsorption on ChCLP in both the systems.

Zeng et al., 2020 performed Cr (VI) removal by using chitosan modified activated carbon derived from *Sargassum horneri* and reported that Freundlich isotherm best fitted in experimental data as compared to Langmuir isotherm. Altun, 2019 reported the Cr (VI) adsorption by using chitosan-coated beads of sour cherry kernel shell and observed the

supremacy of Freundlich isotherm (R^2 = 0.99) over other models that reflected heterogeneous adsorbent surface with multilayer Cr (VI) adsorption. Hasan et al., 2006 investigated Cd (II) adsorption on to chitosan coated perlite beads and reported that Langmuir isotherm best fitted in the Cd (II) adsorption. Shofiyani et al., 2015 reported that adsorption of Cd (II) on to chitosan/chlorella biomass suitably fitted in the Langmuir isotherm, indicating towards monolayer coverage of Cd (II) ions on the adsorbent surface. Park et al., 2015 investigated Cd (II) and Pb (II) adsorption in binary metal ion system on hydroxyapatite/chitosan hybrid. Authors reported that Langmuir isotherm was better fitted as compared to Freundlich isotherm. Dewage et al., 2018 investigated Pb (II) adsorption onto chitosan modified biochar and reported that Langmuir isotherm best fitted in the adsorption as compared to Freundlich.

6.3.3 Thermodynamics

The thermodynamic study of Cr (VI), Cd (II) and Pb (II) of single and ternary metal ion system was performed at varying the temperature (20 to 50 ºC) (Figure 6.16).

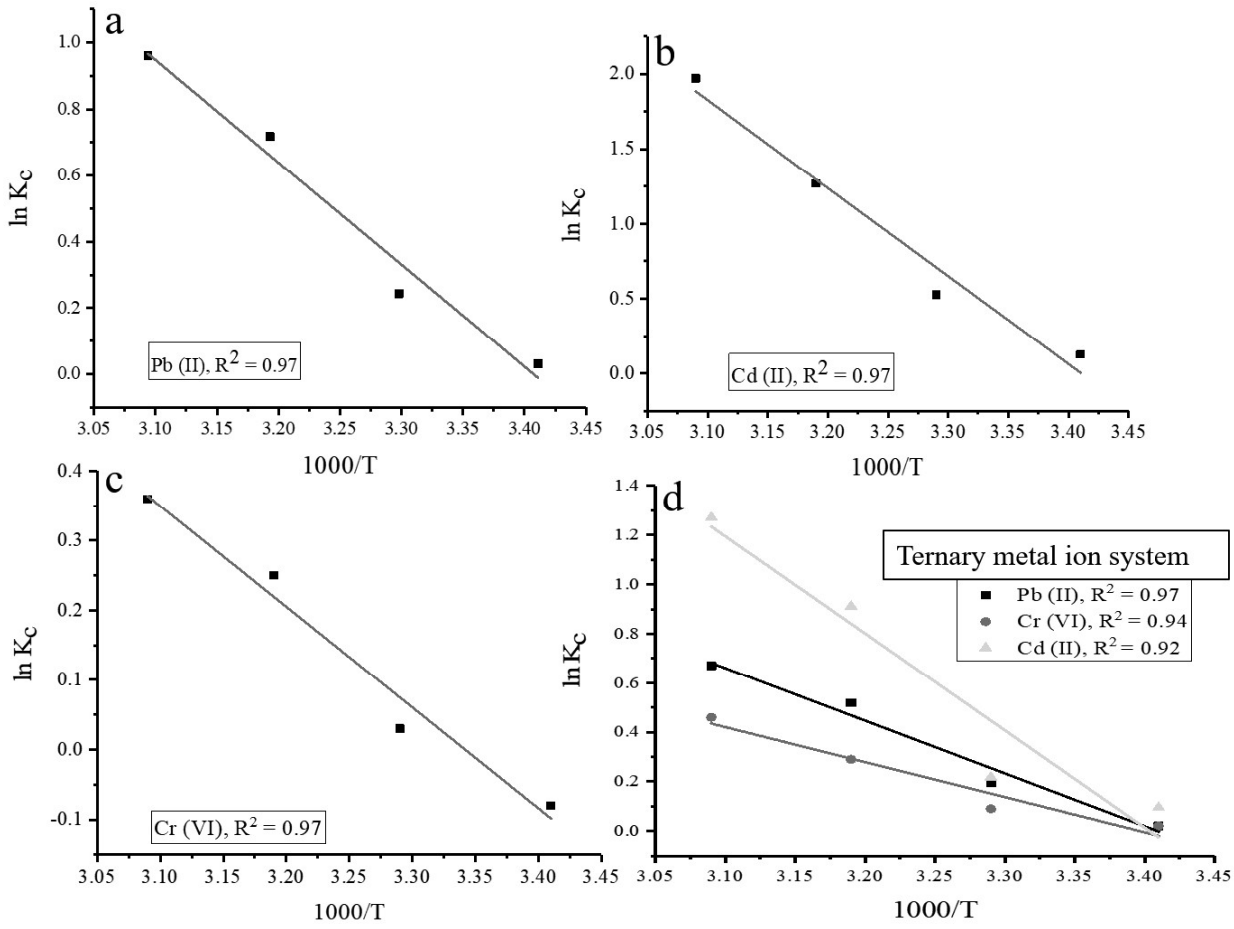

Figure 6.16 Thermodynamics of Pb (II) (**a**), Cd (II) **(b),** Cr (VI) (**c**) adsorption in single and ternary (**d**) metal ions system on ChCLP

The thermodynamic parameters such as ΔH°, ΔG° and ΔS° were calculated for single and ternary metal ion system and tabulated in the Table 6.3 and 6.4.

Table 6.3 Thermodynamic parameters of Cr (VI), Cd (II) and Pb (II) on ChCLP in single metal ion system.

T (°C)	Metal	ΔG^{o} (kJ mol^{-1})	ΔH^{o} (kJ mol^{-1})	ΔS^{o} (J k^{-1} mol^{-1})
20	**Pb (II)**	-75.31	3.08	10.50
30		-614.21		
40		-1871.15		
50		-2579.20		

20	**Cd (II)**	-306.67	5.87	20.04
30		-1331.05		
40		-3309.88		
50		-5295.78		
20	**Cr (II)**	-44.97	1.44	4.83
30		-75.61		
40		-655.03		
50		-967.20		

Table 6.4 Thermodynamic parameters for adsorption of ternary metal ion system

T (ºC)	**Heavy metal**	**ΔG^o (kJ mol^{-1})**	**ΔH^o (kJ mol^{-1})**	**ΔS^o (J k^{-1} mol^{-1})**
20	Pb (II)	-56.05	2.13	7.27
30		-488.19		
40		-1348.62		
50		-1800.06		
20	Cd (II)	231.53	3.93	13.39
30		549.44		
40		2373.11		
50		3412.06		
20	Cr (VI)	-51.18	1.41	4.81
30		-226.83		
40		-755.02		
50		-1235.86		

The positive value of ΔH° in single metal ion system for Cr (VI) (1.44 kJ mol^{-1}), Cd (II) (5.87 kJ mol^{-1}) and Pb (II) (3.08 kJ mol^{-1}), and ternary metal ion system Cr (VI) (1.41 kJ mol^{-1}), Cd (II) (3.93 kJ mol^{-1}) and Pb (II) (2.31 kJ mol^{-1}) pointed towards endothermic heavy metal adsorption on ChCLP coupled with ion-exchange phenomena [Reddy et al. 2012]. The positive value of ΔS° for Cr (VI), Cd (II) and Pb (II) in the single (4.83, 20.00 and 10.50 $JK^{-1}mol^{-1}$) and ternary (4.81, 13.39 and 7.27 $JK^{-1}mol^{-1}$) metal ion system represented the probability of favorable adsorption with amplified randomness at solid liquid interface. The negative values of ΔG° for singe (Table 6.3) and ternary (Table 6.4) metal ion system pointed out spontaneous behavior of adsorption. The ΔG° for both single and ternary metal ion system became more negative with surge in temperature, which indicated that heavy metal adsorption was endothermic. Saha et al., 2013 investigated Cr (VI) removal by using mausmi peel and reported that Cr (VI) adsorption was spontaneous and endothermic. Hussain et al., 2020 investigated thermodynamics of Cd (II) adsorption on spent coffee ground biomass. Authors reported that Cd (II) adsorption was endothermic and spontaneous. Schwantes et al., 2016 performed Cr (III), Cd (II) and Pb (II) adsorption in ternary metal ion system on modified Cassava peels. Authors reported that Cr (II) and Pb (II) adsorption was endothermic, however, Cd (II) adsorption showed exothermic behavior. Authors reported negative values of ΔG° for all three metal ions which indicated towards the spontaneity.

6.3.4 Adsorption kinetic

The kinetic study of Cr (VI), Cd (II) and Pb (II) adsorption was performed for single and ternary metal ion system and graphs are presented in Figure 6.17, 6.18, 6.19 and 6.20.

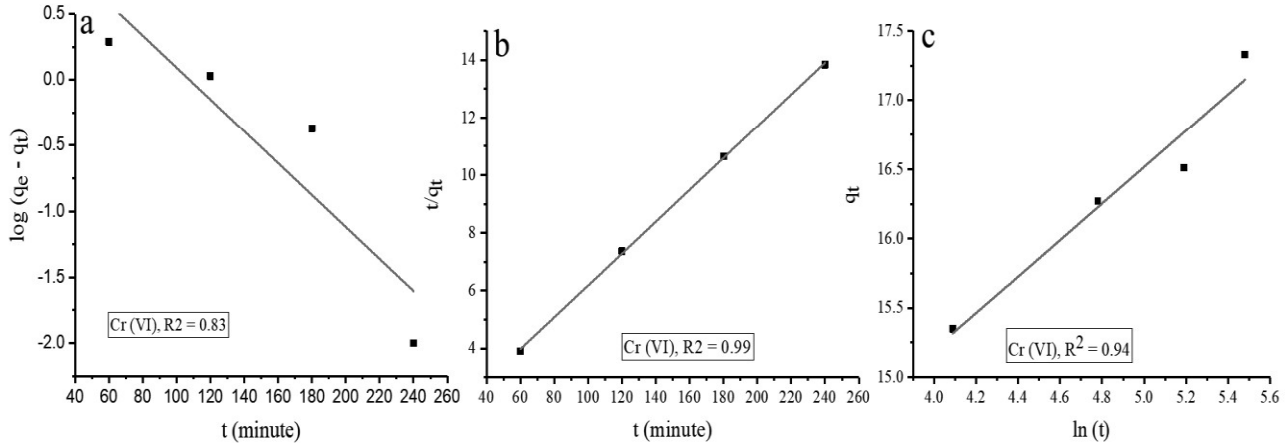

Figure 6.17 PFO (a) and PSO (b) and Elovich (c) kinetic model for Cr (VI) adsorption on ChCLP in single metal ion system

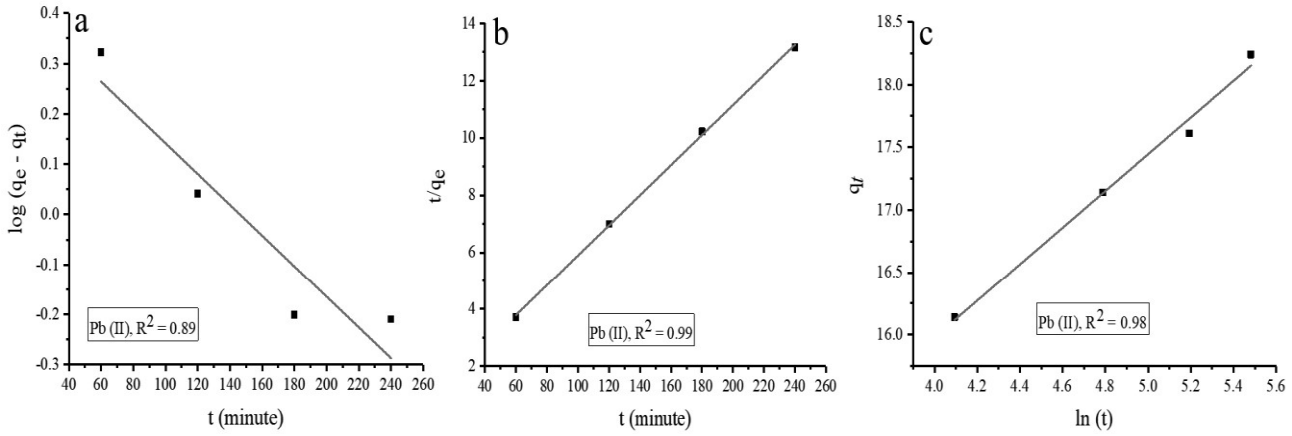

Figure 6.18 PFO (a) and PSO (b) and Elovich (c) kinetic model for Pb (II) adsorption on ChCLP in single metal ion system

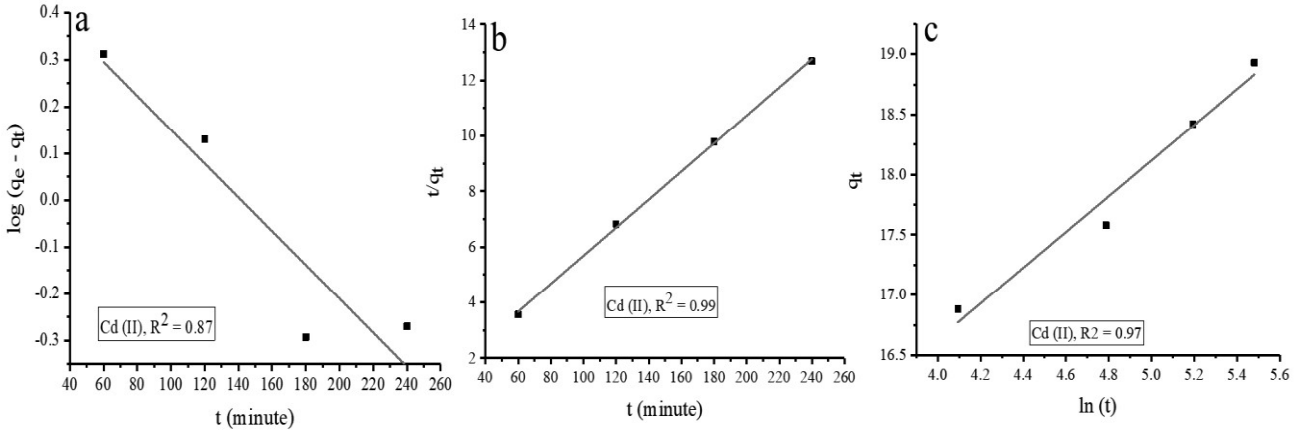

Figure 6.19 PFO (a) and PSO (b) and Elovich (c) kinetic model for Cd (II) adsorption on ChCLP in single metal ion system

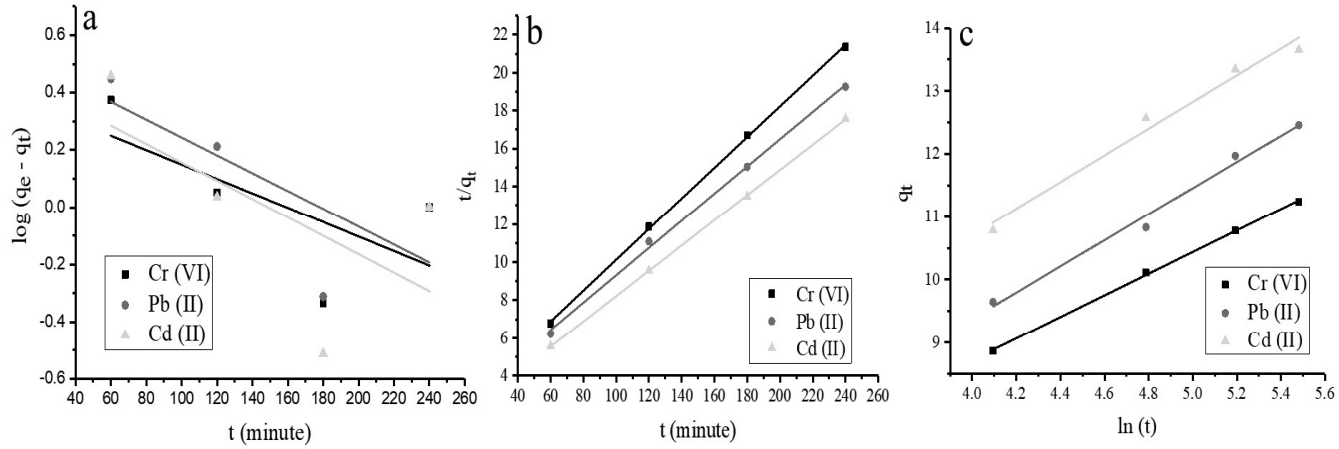

Figure 6.20 PFO (a) and PSO (b) and Elovich (c) kinetic model for adsorption of Cr (VI), Cd (II) and Pb (II) in ternary metal ion system on ChCLP

The kinetic parameters for single and ternary metal ion were calculated from the graphs and tabulated in the Table 6.5 and Table 6.6.

Table 6.5 Kinetic parameters of Cr (VI), Cd (II) and Pb (II) adsorption on ChCLP in single metal ion system

Metal	PFO	PSO	Elovich kinetic

	k_s	q_e	R^2	RSS	k'_2	q_e'	R^2	RSS	α	β	R^2	RSS
Pb (II)	-3.09 $\times 10^{-3}$	0.44	0.89	0.21	0.63	0.05	0.99	0.03	1.46	10.12	0.98	0.20
Cr (VI)	-1.2 $\times 10^{-2}$	1.30	0.83	0.52	0.67	0.06	0.99	0.01	1.31	9.93	0.94	0.10
Cd (II)	-3.4 $\times 10^{-3}$	0.51	0.87	0.41	0.62	0.05	0.99	0.03	1.48	10.69	0.97	0.70

Table 6.6 Kinetic parameters of heavy metal adsorption in ternary metal ion system.

Metal	**PFO**				**PSO**				**Elovich kinetic**			
	k_s	q_e	R^2	RSS	k'_2	q_e'	R^2	RSS	α	β	R^2	RSS
Pb (II)	-3.1 $\times 10^{-3}$	0.55	0.55	0.14	2.12	0.07	0.99	0.01	2.07	1.08	0.98	0.51
Cr (VI)	-2.5 $\times 10^{-3}$	0.40	0.45	0.13	2.02	0.08	0.99	0.05	1.71	1.86	0.98	0.21
Cd (II)	-3.2 $\times 10^{-3}$	0.47	0.39	0.28	1.55	0.06	0.99	4.0× 10^{-3}	2.12	2.20	0.97	0.10

The R^2 value and RSS of PFO, PSO and Elovich kinetic for single (Table 6.5) and ternary metal ion system (Table 6.6) indicated goodness of fit of kinetic model. Higher R^2 and lower RSS value revealed that PSO kinetic model best fitted as compared to PFO and Elovich model in the data of Cr (VI), Cd (II) and Pb (II) in both single and ternary metal ion system. These results also reflected that Cr (VI), Cd (II) and Pb (II) adsorption on ChCLP in single and ternary metal ion system was mediated by chemisorption [Aksu, 2001]. Huang et al., 2016

attempted Cr (VI) adsorption by using beta-cyclodextrin–chitosan modified walnut shell biochar and observed that PSO was well fitted in the adsorption data. Schwantes et al., 2016 reported that PSO best fitted in the Cr (III), Cd (II) and Pb (II) adsorption on chemical modified cassava peels. Shofiyani et al., 2015 investigated Cd (II) adsorption of chitosan-chlorella biomass and reported that PSO kinetic model showed best goodness of fit.

6.3.5 Adsorption Dynamics and diffusivity coefficients

The mechanism of heavy metal adsorption was investigated in the term of dimensionless number and diffusivity coefficients of single and ternary metal ion system. The dimensionless number and diffusivity coefficients were calculated and tabulated in the Table 6.7.

Table 6.7 Value of dimensionless numbers and diffusivity coefficients for metal ions in single and ternary metal ion system.

Heavy metals	**φ**	**λ**	**N_k**	**D_F**	**D_P**
Cr (VI)-single	0.83	2.31×10^{-3}	0.75	4.21×10^{-7}	4.7×10^{-6}
Pb (II)-single	0.87	1.62×10^{-3}	0.71	6.64×10^{-6}	4.7×10^{-6}
Cd (II)-single	0.90	1.00×10^{-3}	0.68	1.16×10^{-6}	4.7×10^{-6}
Cr (VI)-ternary	0.53	4.92×10^{-3}	1.15	8.30×10^{-7}	4.7×10^{-6}
Cd (II)-ternary	0.65	4.33×10^{-3}	0.79	1.40×10^{-6}	4.7×10^{-6}
Pb (II)-ternary	0.59	4.70×10^{-3}	1.04	1.07×10^{-6}	4.7×10^{-6}

Values of the film and pore diffusivity coefficients in Table 6.7 showed that adsorption is dependent upon film diffusion as the values lied between 10^{-6} to 10^{-8} for Cr (VI), Pb (II), Cd (II) in single and ternary metal system. The value of N_k in this study was found to range between 10^{-3} and 10^{1} (Table 6.7), indicating that adsorption was mixed diffusion and transfer controlled. During ternary and single metal ion system, higher values of N_k resulted in greater

adsorption of metal ions, for instance, Cr (VI) and Pb (II) adsorb more in comparison to Cd (II) in both single and ternary metal ion system on the surface of ChCLP. The values of φ and λ were in the range of 10^{-2} to 10^{4} and 10^{-12} to 10^{8}, indicating that ChCLP surface was thoroughly covered during adsorption with reduced surface tension [Joos and Serrien, 1989; Ferri and Stebe, 2000].

6.3.6 ANN Modeling

As network inputs, pH, initial concentration, adsorbent dose, contact time, agitation rate and temperature were employed, with the removal percentage as the target. In order to predict the output function of a feed-forward back-propagation network, the training function TRAINLM was selected, with the transfer function TANSIG together with the Levenberg-Marquardt (L-M) algorithm was applied. The network was trained until the smallest possible number of epochs was attained [Kumar et al., 2019]. After that, the experimental data was integrated with the network simulation to get a final result. A comparison was made between the experimental findings and the predicted output function. Figures 6.21, 6.22, 6.23 and 6.24 illustrate the mean square error (MSE) of the ANN model acquired during data training, testing and validation for Cr (VI), Cd (II), and Pb (II) ions in single and ternary metal system, respectively. The L-M algorithm produced the lowest mean square error during data training, testing, and validation (encircled point). In the present study, the L-M algorithm was concluded appropriate for predicting the output function with the lowest MSE at epoch (14, 2 and 4 for Cr (VI), Cd (II) and Pb (II) ions in single metal system) and epoch 0 for ternary metal system. It was coupled with highest validation performance in ten neurons at 8.6688, 7.0701, 16.9923 for Cr (VI), Cd (II), Pb (II) ions in single metal system and 0.0043892 for ternary metal system, respectively (Figures 6.21, 6.22, 6.23, and 6.24).

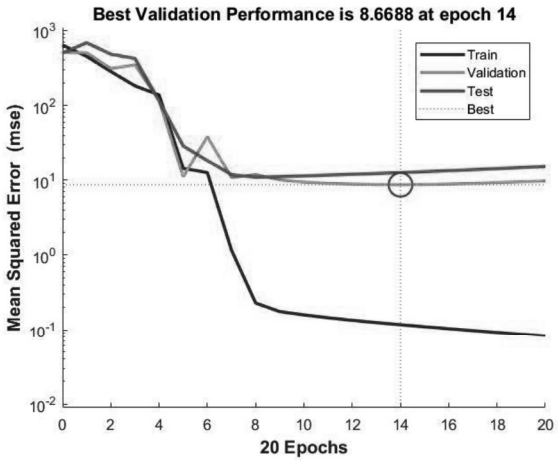

Figure 6.21 Performance between number of epochs and the MSE for Cr (VI) ions in single metal system

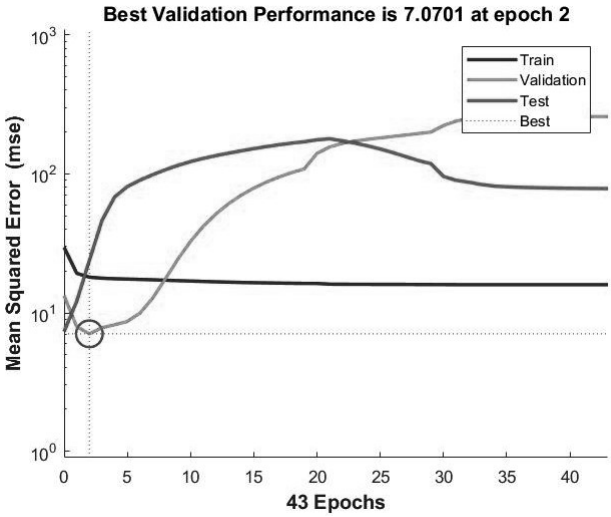

Figure 6.22 Performance between number of epochs and the MSE for Cd (II) ions in single metal ion system

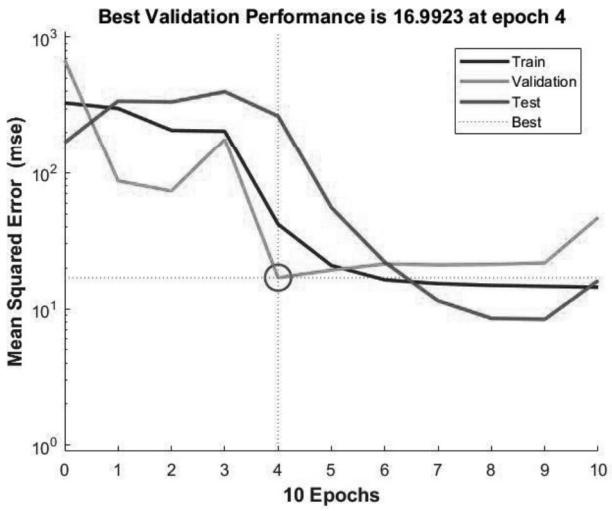

Figure 6.23 Performance between number of epochs and the MSE for Pb (II) ions in single metal ion system

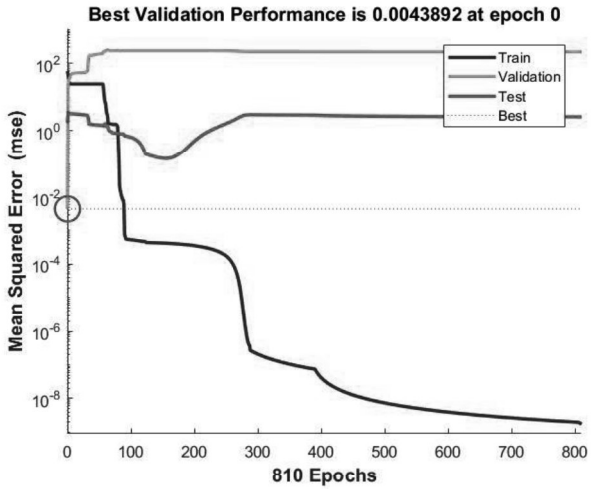

Figure 6.24 Performance between number of epochs and the MSE for ternary metal ion system

Figure 6.25, 6.26 and 6.27 shows regression between experimental and predicted values for the adsorption of Cr (VI), Cd (II), Pb (II) ions in single metal ion system and Figure 6.28 in ternary metal ion system. The circles in the plot are experimental values and the colored lines show the predicted values derived from the ANN models. Both the experimental and theoretical values seemed to be in agreement with each other showing a high regression coefficient (R^2 = 0.99) for Cr (VI), 0.92 for Cd (II) and 0.94 for Pb (II) in single metal ion

system (Figure 6.25, 6.26 and 6.27) and R^2 of 0.86 i.e., comparatively low in ternary metal ion system (Figure 6.28).

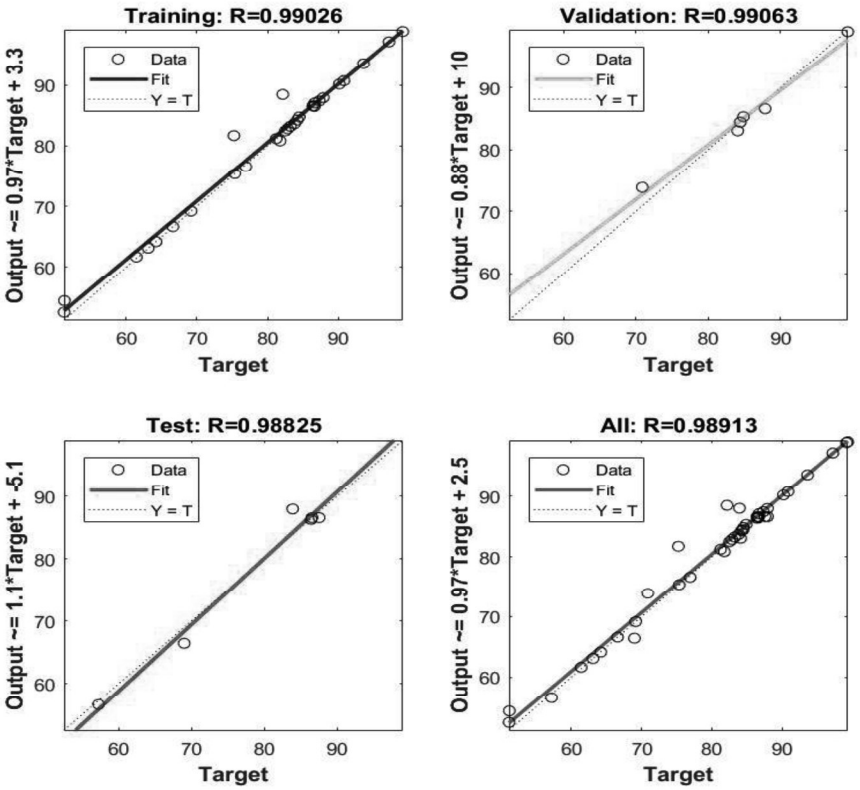

Figure 6.25 Regression plot for Cr (VI) ions in single metal ion system

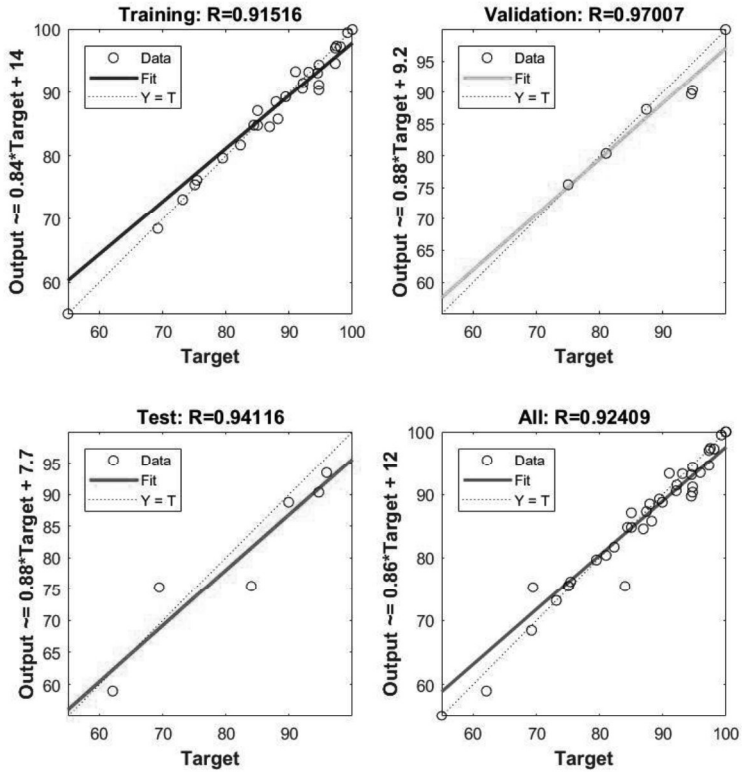

Figure 6.26 Regression plot for Cd (II) ions in single metal ion system

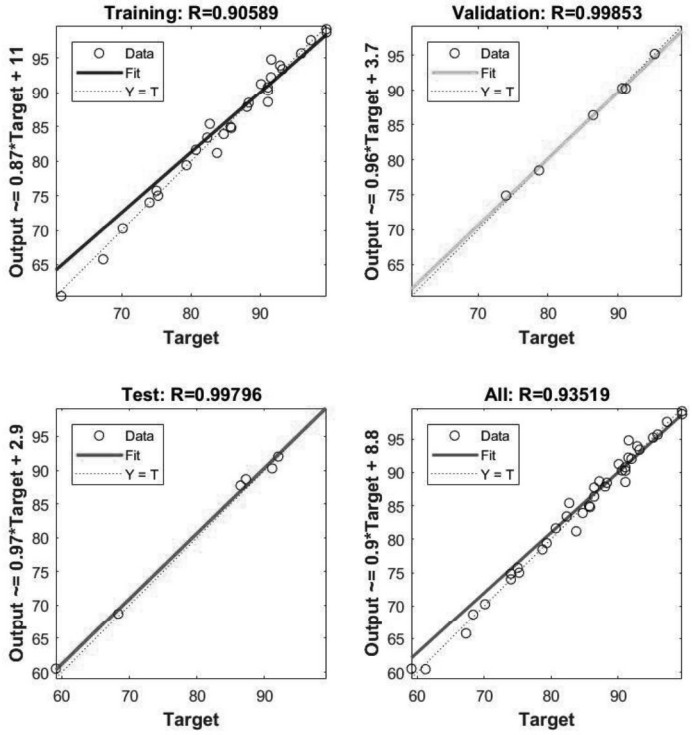

Figure 6.27 Regression plot for Pb (II) ions in single metal ion system

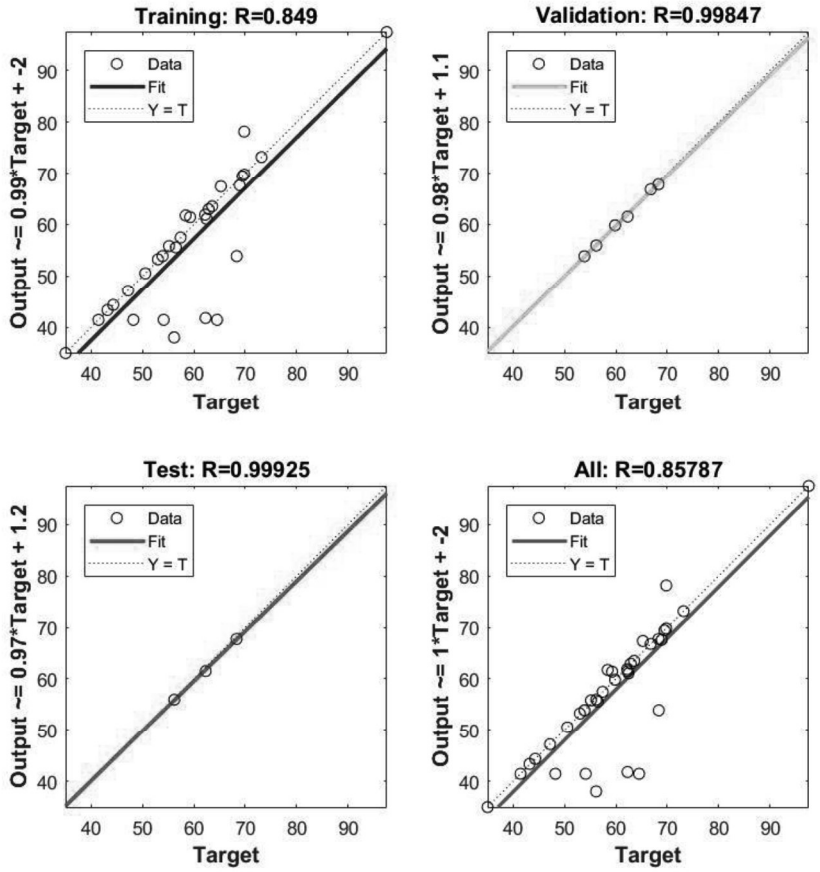

Figure 6.28 Regression plot for ternary metal ion system

The correlation plot showed high regression coefficient (0.98) for Cr (VI), 0.90 for Cd (II), 0.91 for Pb (II) ions in single metal ion system and for ternary metal ions solution, the R^2 was 0.98 for Cr (VI), 0.94 for Cd (II), 0.72 for Pb (II) ions between the experimental and predicted values. The results also showed a small deviation of 0.40% for Cr (VI), 0.59% for Cd (II), 0.52% for Pb (II) ions in single and for ternary metal ion system; 1.08% for Cr (VI), 0.51% for Cd (II), 4.61% for Pb (II) ions between the experimental and predicted values (Figure 6.29, 6.30, 6.31 and 6.32).

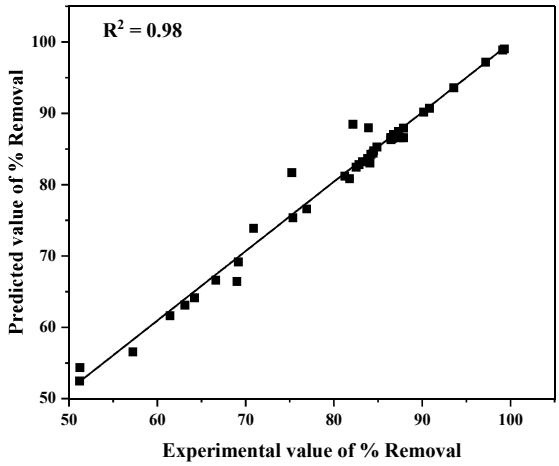

Figure 6.29 Correlation plot for the experimental and ANN predicted values for Cr (VI) ions in single metal ion system

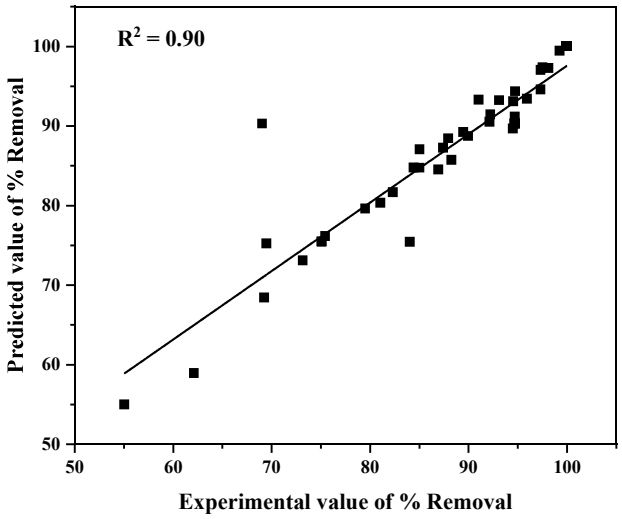

Figure 6.30 Correlation plot for the experimental and ANN predicted values for Cd (II) ions in single metal ion system

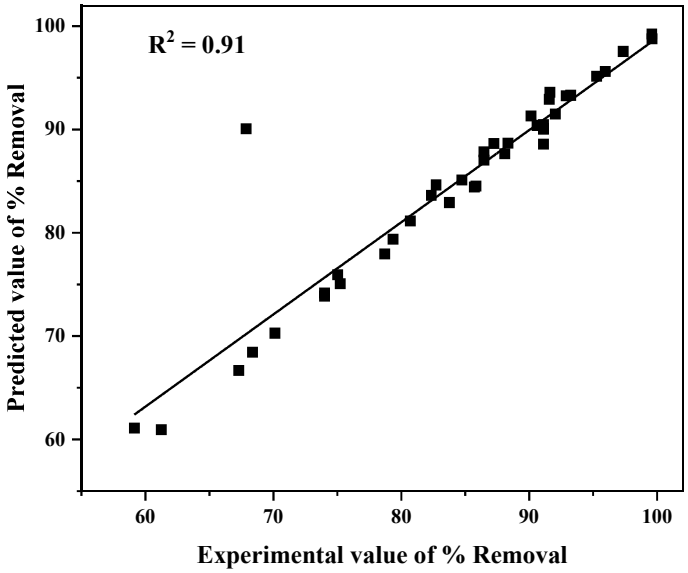

Figure 6.31 Correlation plot for the experimental and ANN predicted values for Pb (II) ions in single metal ion system

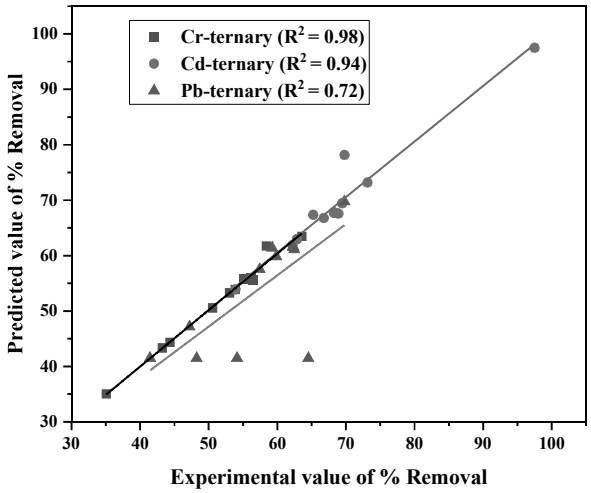

Figure 6.32 Correlation plot for the experimental and ANN predicted values for ternary metal system

The higher deviation of ternary metal system results with lower regression coefficient was observed in Figure 6.28. This further showed the suitability of L-M algorithm for both single and ternary metal ions system in the present work.

Narayana et al., 2021 used artificial neural networks modelling to remove lead from aqueous solutions utilizing bio-waste-derived iron oxide nano composites. Their goal is to create an artificial neural network (ANN) model that can estimate and assess the link between Pb (II) removal and process parameters. The back propagation algorithm was used to train the model. With new unseen datasets, the model was validated. The R^2 value for the whole datasets is 0.991. Sensitivity analysis and the establishment of a simulated adsorption were used to investigate the link between the parameters and Pb (II) removal. The researchers [Narayana et al., 2021] discovered that ANN modelling was a good technique for predicting and optimizing adsorption process parameters for maximum Pb (II) removal. With the use of green adsorbent, Mitra et al., 2019 were able to observe the smallest possible MSE (0.000167 for Cr (VI) and 4.20 105 for Pb (II), which corresponds to the pruning process. The extremely low values of all of the statistical error parameters imply that the final prediction was correct in terms of the final outcome. It is obvious from the findings that the ANN model is capable of accurately predicting the percentage removal. Additionally, Amouei et al., 2013 conducted a study on the removal of cadmium from aqueous solutions by sunflower powder and did modelling of the process using ANN. The data were modelled by using a neural network with four hidden neurons. Contact time and initial concentration were used as input factors, whereas an adsorbed pollutant was used as an output variable. For each series of adsorption data, the upper and lower initial concentrations were provided as the training data set for fitting the initial concentration dependent neural network, while the remaining series (intermediate initial concentration) served as the validation data set for evaluating the neural network predictions for the data that

were not used during the fitting process. It has been observed that neural network model predicted the observed data points quite well for both the training and validation data sets. Thus in the present work, ANN was observed as an excellent tool for modelling and optimizing Cr (VI), Cd (II) and Pb (II) removal with low mean square error and a high correlation coefficient, which is consistent with the work reported by other researchers [Narayana et al., 2021; Mitra et al., 2019; Amouei et al., 2013].

6.4.0 Complete removal of heavy metal ions in series batch reactor system

ChCLP has high heavy metal removal capacity 99.34 % Cr (VI), 99.92 % Cd (II) and 99.58 % Pb (II) at 100 mg/L initial metal ion concentration and 10 g/L ChCLP dosage. However, 0.66 mg/L Cr (VI), 0.08 % Cd (II) and 0.42 % Pb (II) were left in the water. This residual amount of Cr (VI), Cd (II) and Pb (II) were much higher than the permissible limit of their discharge Cr (VI) (0.05 mg/L), Cd (II) (0.003 mg/L) and Pb (II) (0.01 mg/L) as demarcated by WHO, USA. Thereby, residual heavy metals were eliminated by re-treatment of first step's effluent into second batch reactor configured in series. The experiment setup of batch reactors arranged in series is shown in Figure 6.33.

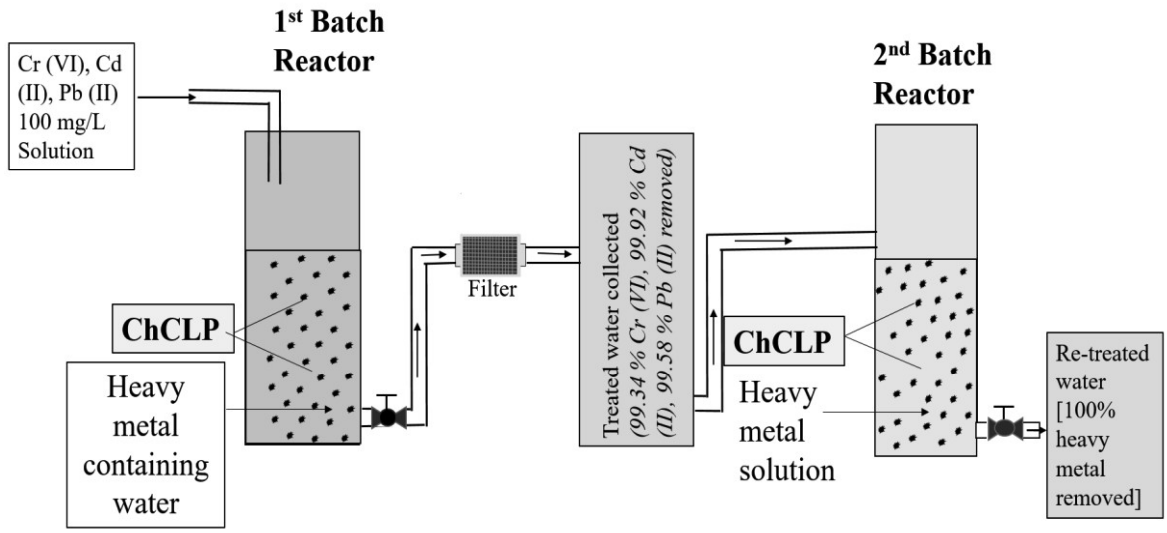

Figure 6.33 Diagrammatic demonstration of heavy metal removal in series batch reactor system

After second round treatment, 100% Cr (VI), Cd (II) and Pb (II) removal was obtained. The water treated in second round meets with permissible limit of heavy metal ion discharge in the water. ChCLP biomass showed emerging application for removal of Cr (VI), Cd (II) and Pb (II) from wastewater.

6.5.0 Regeneration of chitosan coated ChCLP

An ideal adsorbent can be utilized in the multiple adsorption-desorption cycles. Desorption of the heavy metal ions from the biosorbent was studied by solvent elution method. Desorption experiment was performed using 0.10 M HNO_3 as stripping agent. 0.10 g of metal ions loaded dried biosorbent was mixed with the 50 ml 0.10 M HNO_3 and incubated for 1 hour at room temperature. After incubation, the solution was filtered and metal ions concentration was measured. The % desorption was calculated by Equation 32

$$\% \text{ Desorption} = \frac{100[C_D V_D]}{q_{em}} \tag{32}$$

where, C_D is metal ion concentration (mg/L) in the desorbed solution, V_D is desorbed solution volume in Litre (L), m is mass (g) of biosorbent and q_e (mg/g) is biosorption capacity. The five cycle of adsorption-desorption was performed to estimate reusability of the biosorbent. At the end of each cycle, biosorbent were washed with double distilled water and dried in oven at 105 ºC. The adsorption-desorption capacity of ChCLP over the five cycles is shown in the Figure 6.34, 6.35 and 6.36**.**

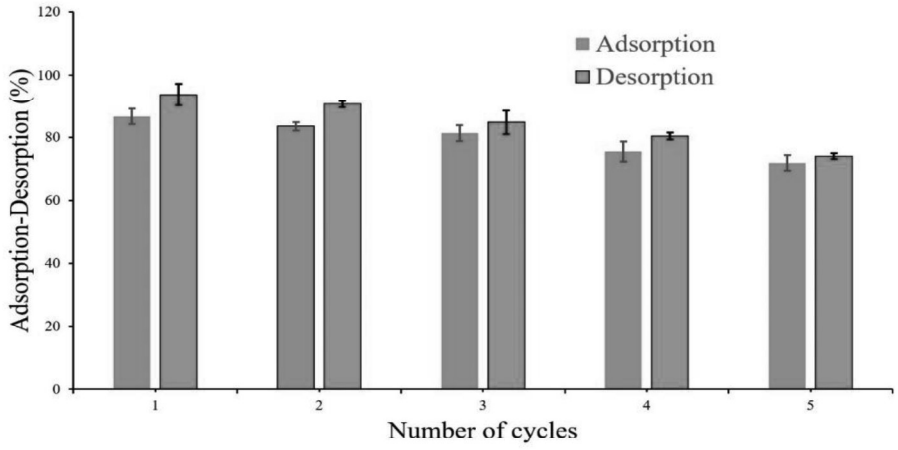

Figure 6.34 Adsorption and desorption of Cr (VI) on ChCLP

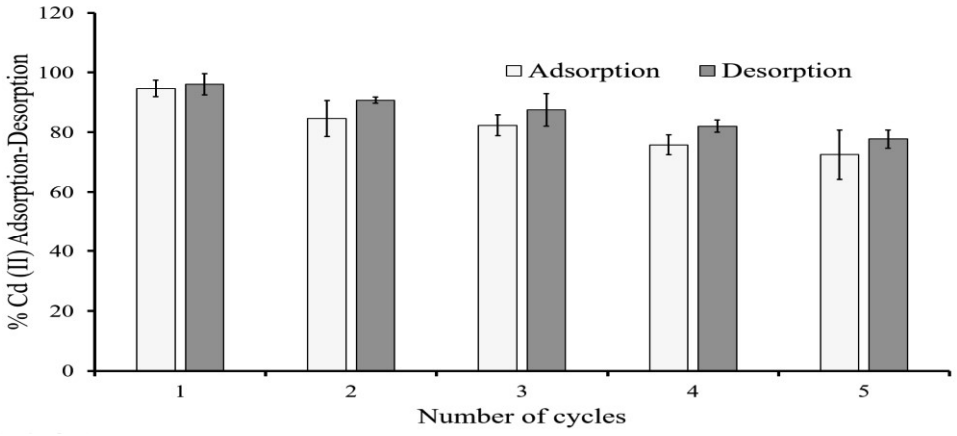

Figure 6.35 Adsorption and desorption of Cd (II) on ChCLP

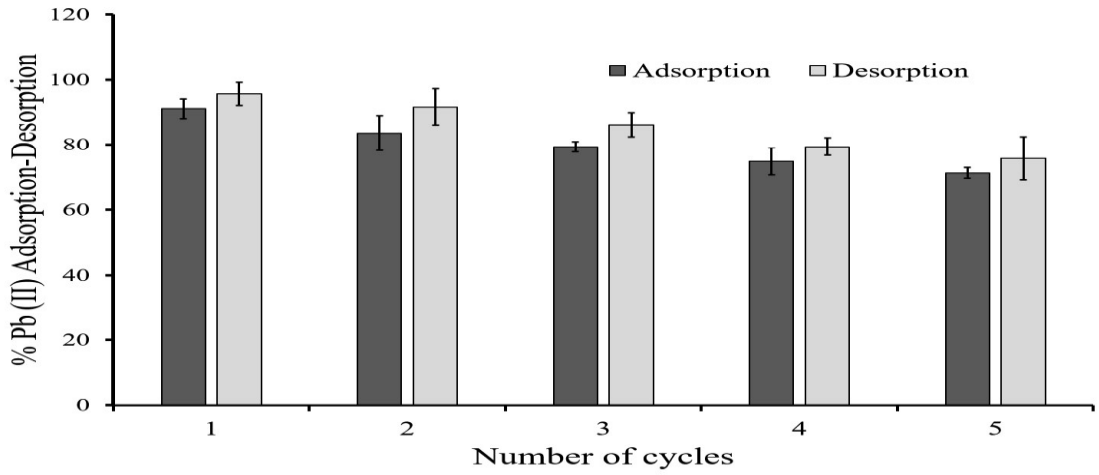

Figure 6.36 Adsorption and desorption of Pb (II) on ChCLP

The removal of Cr (VI), Cd (II) and Pb (II) on ChCLP decreased from 86.65 to 71.89 % (Figure 6.34), 94.69 to 72.59 % (Figure 6.35) and 91.12 to 71.22 % (Figure 6.36), respectively in 1st to 5th adsorption-desorption cycles. The decrement in the heavy metal adsorption after five times regeneration cycles was due to deactivation of metal binding sites on ChCLP surface. The better adsorption capacity after several regeneration cycles indicates that ChCLP is a good and potential biosorbent. There was deactivation of active sites on account of repeated washing, reagents used in the elution and binding of unwanted impurities

with active sites. The % desorption decreased of Cr (VI), Cd (II) and Pb (II) from 93.78 to 74.10, 96.08 to 77.77 and 95.78 to 75.77, respectively. This was due to strong binding of heavy metal ions with ChCLP. Liu et al. 2021 also performed five cycles of regeneration experiment and reported that Cr (VI) removal efficiency decreased from 72.8% to 65.2% (100 mg/L) at end of the fifth cycle. Bayuo et al., 2020 investigated desorption efficiency of Cr (VI) and Pb (II) on groundnut husk and reported that it was reduced up to 20.0 % for Cr (VI) and 26.70 % Pb (II) after three cycles. Pandey et al., 2007 investigated Cr (VI), Pb (II) and Cu (II) adsorption-desorption on calcium alginate and reported that desorption of Cr (VI), Pb (II) and Cu (II) was decreased up to 3 %, 14 % and 15 %, respectively.

6.6 Techno-economic analysis

The cost analysis is a primary approach of scaling up the heavy metal treatment process [Santos-Juanes Jorda et al., 2011; Fawzy et al., 2018]. The cost estimation procedure is meaningful in the design water treatment systems [Hamdy et al., 2018]. In the present study the production cost of adsorbent (ChCLP) was estimated. The operation cost per cubic meter of water treatment was calculated through sum of chemicals/reagents and biosorbent cost. The cost/price of adsorbent preparation can be calculated as:

P_i ($USD/g) = Raw materials cost + chemicals/regents + adsorbent preparation cost

The operation cost for treatment of heavy metal ions was calculated using following Equation

$$\text{Operation cost } (\$USD/m^3) = C_i \times P_i$$

where, C_i (g/m^3) is the concentration of adsorbent and P_i ($USD/g) is price of adsorbent.

In this present study, the cost of ChCLP was calculated 0.26 as $USD/g which used for the removal of Cr (VI), Cd (II) and Pb (II) from water and 0.5 g ChCLP used for the treatment of 1 litre of water. The operation cost of ChCLP mediated heavy metal treatment was calculated and observed as 130 $USD/$m^3$. Fawzy Et al., 2019 prepared adsorbent using Olive leaves for removal of Cr (II) and investigated the techno-economic analysis. Authors reported similar kind of results in their research.

6.7.0 Conclusion

The ChCLP was synthesized from chitosan and *Citrus limetta* peel biomass. ChCLP surface was rough and porous spiked with functional groups such as hydroxyl, amide and carboxyl. The presence of C, N and O demonstrated the chitosan coating on ChCLP. 86.69 % Cr (VI), 94.69 % Cd (II) and 91.12 % Pb (II) removal was reported at 100 mg/L and 5 g/L ChCLP dosage. On other hand, the *Citrus limetta* peel (CLP) has a lower heavy metal removal capacity than ChCLP for example 72.12 % Cr (VI), 77.09 % Cd (II) and 73.67 % Pb (II) at 100 mg/L initial metal ion concentration. The heavy metal removal pattern of Cr (VI), Cd (II) and Pb (II) followed as Cd (II) > Pb (II) > Cr (II). The surface morphology of ChCLP showed porous and rough surface. It became more porous and rough after chitosan coating which was observed in SEM and AFM analysis. The chitosan coating and adsorption of heavy metal ions was confirmed by EDX, XPS and elemental mapping. The adsorption data of Cd (II) and Pb (II) adsorption of both single and ternary metal ion system was best fitted in the Langmuir isotherm which indicated towards monolayer adsorption on homogeneous adsorbent surface. Cr (VI) adsorption of single and ternary metal ion system was suitably fitted into Freundlich isotherm, showing multilayer adsorption on heterogeneous surface. PSO kinetic model best fitted in the adsorption data of all three metal ions in both single and ternary metal ion system which denoted chemisorptive mode of adsorption. Adsorption of Cr (VI), Cd (II) and Pb (II) was mix diffusion and transfer controlled for both single and ternary metal ion system. The LM algorithm produced the lowest MSE values, 8.6688, 7.0701, 16.9923, and 0.0043892, as well as the largest R^2 values, 0.99, 0.92, 0.94, and 0.86, for the prediction of percentage removal of Cr (VI), Cd (II), and Pb (II) ions in single and ternary metal ion system, respectively. As a result, it was determined to be the most effective training algorithm. According to the results of the ANN, neural network modelling may be utilized to effectively simulate and predict percentage removal. Thermodynamic study revealed that heavy metal adsorption in single and

ternary metal ion system was endothermic, spontaneous and favourable. The ChCLP can be utilized in the several adsorption-cycles. The 100 % heavy metal removal was achieved in series reactor treatment system, which removed heavy metal concentration below the permissible limit of discharge as demarcated by WHO, USA.